Hindawi Publishing Corporation
Advances in Electrical Engineering
Volume 2014, Article ID 482805, 25 pages
http://dx.doi.org/10.1155/2014/482805

Review Article

Filter Bank Multicarrier Modulation: A Waveform Candidate for 5G and Beyond

Behrouz Farhang-Boroujeny

ECE Department, University of Utah, Salt Lake City, UT 84112, USA

Correspondence should be addressed to Behrouz Farhang-Boroujeny; farhang@ece.utah.edu

Received 7 August 2014; Accepted 11 November 2014; Published 21 December 2014

Academic Editor: Gorazd Stumberger

Recent discussions on viable technologies for 5G emphasize on the need for waveforms with better spectral containment per subcarrier than the celebrated orthogonal frequency division multiplexing (OFDM). Filter bank multicarrier (FBMC) is an alternative technology that can serve this need. Subcarrier waveforms are built based on a prototype filter that is designed with this emphasis in mind. This paper presents a broad review of the research work done in the wireless laboratory of the University of Utah in the past 15 years. It also relates this research to the works done by other researchers. The theoretical basis based on which FBMC waveforms are constructed is discussed. Also, various methods of designing effective prototype filters are presented. For completeness, polyphase structures that are used for computationally efficient implementation of FBMC systems are introduced and their complexity is contrasted with that of OFDM. The problems of channel equalization as well as synchronization and tracking methods in FBMC systems are given a special consideration and a few outstanding research problems are identified. Moreover, this paper brings up a number of appealing features of FBMC waveforms that make them an ideal choice in the emerging areas of multiuser and massive MIMO networks.

1. Introduction

In the past, orthogonal frequency division multiplexing (OFDM) has enjoyed its dominance as the most popular signaling method in broadband wired [1, 2] and wireless [3, 4] channels. OFDM has been adopted in the broad class of DSL standards as well as in the majority of wireless standards, for example, variations of IEEE 802.11 and IEEE 802.16, 3GPP-LTE, and LTE-Advanced. OFDM is known to be a perfect choice for point-to-point communications, for example, from a base station to a mobile node and vice versa. It offers a minimum complexity and achieves very high bandwidth efficiency. However, it has been noted that OFDM has to face many challenges when considered for adoption in more complex networks. For instance, the use of OFDM in the uplink of multiuser networks, known as OFDMA (orthogonal frequency division multiple access), requires full synchronization of the users' signals at the base station input. Such synchronization was found to be very difficult to establish, especially in mobile environments where Doppler shifts of different users are hard to predict/track. Morelli et al. [5] have noted that carrier and timing synchronization represents the most challenging task in OFDMA systems. To combat the problem, some researchers have relaxed on the need for a close to perfect carrier synchronization among users and have proposed multiuser interference cancellation methods [6–9]. These methods are generally very complex to implement. Their implementation increases the receiver complexity by orders of magnitude [10]. Hence, one of the main advantages of OFDM, the low complexity, will be lost.

Another limitation of OFDM appears when attempt is made to transmit over a set of noncontiguous frequency bands, known as *carrier aggregation*. The poor response of the subcarrier filters in IFFT/FFT filter banks of OFDM introduces significant out-of-band *egress noise* to other users and also picks up significant *ingress noise* from them. The same problem appears if one attempts to adopt OFDM for filling in the spectrum holes in cognitive radios. Methods of reducing OFDM spectral leakage prove to be very limited in performance and may add significant complexity to

the transmitter. For instance, the side lobe suppression techniques, like those proposed in [11–13], can achieve an out-of-band emission suppression of only 5 to 10 dB, while they may add significant complexity to the transmitter and they will incur some loss in bandwidth efficiency.

Filter bank multicarrier (FBMC) is an alternative transmission method that resolves the above problems by using high quality filters that avoid both ingress and egress noises. Also, because of the very low out-of-band emission of subcarrier filters, application of FBMC in the uplink of multiuser networks is trivial [14, 15]. It can be deployed without synchronization of mobile user nodes signals. In the application of cognitive radios, the filter bank that is used for multicarrier data transmission can also be used for spectrum sensing [16–20]. On the other hand, compared to OFDM, FBMC falls short in handing multiple-input multiple-output (MIMO) channels, although a few solutions to adopt FBMC in MIMO channels have been reported in the literature; for example, see [21–23]. Nevertheless, as our recent research study has shown (see Section 8, below), in the emerging area of *massive* MIMO, FBMC is found as powerful as OFDM and in some cases superior to OFDM.

In the past, many attempts have been made to adopt FBMC in various standards. Apparently, the earliest proposal to use FBMC for multicarrier communications is a contribution from Tzannes et al. of AWARE Inc., in one of the asymmetric digital subscriber lines (ADSL) standard meetings in 1993 [24]. The proposed method that was called discrete wavelet multitone (DWMT) was further studied in [25, 26]. Despite enthusiasm from the research community (see [27] and the cited references therein), DWMT was not adopted in the ADSL standard. This was partly because of the perceived complexity of this method as compared to its rival, DMT (discrete multitone, an equivalent name for OFDM in DSL literature). Indeed, the DWMT structure proposed by Tzannes et al. was significantly more complex than that of DMT. The major part of the complexity of DWMT came from the equalization method that was adopted. The detailed discussion presented in [26] assumed that one needs an equalizer that combines signals from each subcarrier band and its adjacent bands. Typical equalizer lengths suggested in [26] were 21 real-valued taps per subcarrier. It was later noted by the author of this paper that if each subcarrier is sufficiently narrow such that it can be approximated by a flat gain, two real taps per subcarrier would be sufficient for equalization [27]. This observation led to further study of DWMT. In power line communications (PLC) community, it has been named wavelet OFDM and was adopted in the IEEE P1901 standard [28]. The main motivation for use of DWMT in DSL and its adoption later in PLC was to deal with ingress and egress noises, since both DSL and PLC use unshielded copper lines that are subject to strong radio interference. Moreover, in 1999, an FBMC method with nonoverlapping subcarrier bands was proposed as a solution for filtering the narrow-band interferences in very high-speed DSL (VDSL) channels [29]. The proposed method was called filtered multitone (FMT). This proposal that was included as an annex in one of the initial draft documents of VDSL [30] was further developed by a number of researchers [31–34]. However, to avoid incompatibility with ADSL, FMT was not included in the final document of the VDSL standard [35]. Another unsuccessful story is an attempt by France Telecom [36] to introduce FBMC in the IEEE 802.22, a cognitive radio standard to access TV bands in wireless rural area networks (WRAN). Up to now, apparently, the only standard for radio transmission that uses FBMC is the TIAs Digital Radio Technical Standard [37].

Recent discussions on the fifth generation (5G) wireless communications have initiated a much stronger wave of interest in deviating from the main stream of OFDM systems. This shift of interest is clearly due to limitations of OFDM in the more dynamic and multiuser networks of future. A number of proposals have been made to adopt new waveforms with improved spectral containment. A good example of such activity is the 5GNOW project in Europe which challenges LTE and LTE-Advanced in coping with the dynamic needs of 5G. The 5GNOW has identified four alternative choices of waveforms to better serve 5G needs. These waveforms that are all built based on some sort of filtering may be thought as adoptions of FBMC method to suit different needs of various applications. We refer interested readers to the documents available at http://www.5gnow.eu for the details of the proposed waveforms by the 5GNOW group. Another major activity that has performed a broad study of FBMC is due to the PYHDYAS project (also in Europe). The PHYDYAS contributors have published heavily on various aspects of FBMC, including prototype filter design, equalization, synchronization, and application to MIMO channels. A summary of the major findings of the PHYDYAS contributors is presented in [21], and a complete list of their publications can be found at http://www.ict-phydyas.org.

The main thrust of this paper is to present a point of view of FBMC and its future applications as seen by the author. While we acknowledge the presence of a large body of works on FBMC, the paper details are geared towards the research outcomes of the author and his students in past 15 years. The paper emphasis is on the recent works of the author and his students. Many shortcomings of OFDM in dealing with the requirement of the next generation of wireless systems are discussed and it is shown how FBMC overcomes these problems straightforwardly. We present a derivation of FBMC systems that reveals the relationships among different forms of FBMC. A method of designing FBMC systems for a near-optimum performance in doubly dispersive channels is presented and its superior performance over OFDM is shown. The example considered is an underwater acoustic channel. Application of FBMC technique to massive MIMO communications is introduced and its advantages in this emerging technology are revealed. Last, but not the least, the problems of channel equalization and synchronization in FBMC systems are also given a special treatment and a number of outstanding research problems in this field, for future studies, are identified.

This paper begins with a historical overview of FBMC methods in Section 2. In order to keep the presentation in this paper a complement to those we have recently reported in [19, 38], the rest of this paper is organized as follows. A summary of the theoretical background based on which the various

forms of FBMC are built are presented in Section 3. Methods of designing prototype filters for FBMC are presented in Section 4. Polyphase structures that are used for efficient implementation of FBMC systems are reviewed in Section 5. A few comments on complexity comparison of FBMC and OFDM are also made in this section. Channel equalization in FBMC systems is discussed in Section 6. Methods of carrier and symbol timing acquisition and tracking in FBMC systems are reviewed in Section 7. Here, a few particular features of FBMC systems that need special attention for their successful implementation are highlighted. Section 8 reminds the reader of a number of applications in the literature where FBMC has been found to be a good fit. This section also discusses the opportunities offered by FBMC in the emerging area of massive MIMO. The concluding remarks of the paper are made in Section 9.

Notations. The presentations in this paper follow a mix of continuous-time and discrete-time formulations, as appropriate. While $x(t)$ refers to a continuous function of time, t, $x[n]$ is used to refer to its discrete-time version, with n denoting the time index. The notation f is used as frequency variable in $X(f)$, the Fourier transform of the continuous-time signal $x(t)$, and also as normalized frequency in $X(e^{j2\pi f})$, the Fourier transform of the discrete-time signal $x[n]$. We use $\star$ to denote linear convolution, and the superscript $*$ to denote complex conjugate.

2. Review of FBMC Methods

FBMC communication techniques were first developed in the mid-1960s. Chang [39] presented the conditions required for signaling a parallel set of PAM symbol sequences through a bank of overlapping filters within a minimum bandwidth. To transmit PAM symbols in a bandwidth-efficient manner, Chang proposed vestigial sideband (VSB) signaling for subcarrier sequences. Saltzberg [40] extended the idea and showed how Chang's method could be modified for transmission of QAM symbols in a double-sideband- (DSB-) modulated format. In order to keep the bandwidth efficiency of this method similar to that of Chang's signaling, Saltzberg noted that the in-phase and quadrature components of each QAM symbol should be time staggered by half a symbol interval. Efficient digital implementation of Saltzberg's multicarrier system through polyphase structures was first introduced by Bellanger and Daguet [41] and later studied by Hirosaki [42, 43]. Another key development appeared in [44], where the authors noted that Chang's/Saltzberg's method could be adopted to match channel variations in doubly dispersive channels and, hence, minimize intersymbol interference (ISI) and intercarrier interference (ICI).

Saltzberg's method has received a broad attention in the literature and has been given different names. Most authors have used the name offset QAM (OQAM) to reflect the fact that the in-phase and quadrature components are transmitted with a time offset with respect to each other. Moreover, to emphasize the multicarrier feature of the method, the suffix OFDM has been added, hence, the name OQAM-OFDM. Others have chosen to call it staggered QAM (SQAM), equivalently SQAM-OFDM. In [38] we introduced the shorter name staggered multitone (SMT).

Chang's method [39], on the other hand, has received very limited attention. Those who have cited [39] have only acknowledged its existence without presenting much detail, for example [41, 45, 46]. In particular, Hirosaki who has extensively studied and developed digital structures for the implementation of Saltzberg's method [43, 47] has made a brief reference to Chang's method and noted that since it uses VSB modulation, and thus its implementation requires a Hilbert transformation, it is more complex to implement than Saltzberg's method. This statement is inaccurate, since as we have demonstrated in [38] Chang's and Saltzberg's methods are equivalent and, thus, with a minor modification, an implementation for one can be applied to the other. More on this is presented in Section 5. Also, as noted earlier, a vast literature in digital signal processing has studied a class of multicarrier systems that has been referred to as DWMT. It was later noted in [27, 48] that DWMT uses the same analysis and synthesis filter banks as the cosine modulated filter banks (CMFB) [49]. CMFB, on the other hand, may be viewed as a reinvention of Chang's method, with a very different application in mind [38]. In [38], we also introduced the shorter name cosine modulated multitone (CMT) to be replaced for DWMT and/or CMFB.

One more interesting observation is that another class of filter banks which were called modified DFT (MDFT) filter bank has appeared in the literature [50]. Careful study of MDFT reveals that this, although derived independently, is in effect a reformulation of Saltzberg's filter bank in discrete-time and with emphasis on compression/coding. The literature on MDFT begins with the pioneering works of Fliege [51] and later has been extended by others, for example [52–55].

Finally, before we proceed with the rest of our presentation, it should be reiterated that we identified three types of FBMC systems: (i) CMT: built based on the original idea of Chang [39]; (ii) SMT: built based on the extension made by Saltzberg [40]; and (iii) FMT: built based on the conventional method frequency division multiplexing (FDM) [34].

3. Theory

The theory of FBMC, particularly those of CMT and SMT, has evolved over the past five decades by many researchers who have studied them from different angles. Early studies by Chang [39] and Saltzberg [40] have presented their finding in terms of continuous-time signals. The more recent studies have presented the formulations and conditions for ISI and ICI cancellation in discrete-time, for example, [46, 50]. On the other hand, a couple of recent works [19, 38], from the author of this paper and his group, have revisited the more classical approach and presented the theory of CMT and SMT in continuous time. It is believed that this formulation greatly simplifies the essence of the theoretical concepts behind the theory of CMT and SMT and how these two waveforms are related. It also facilitates the design of prototype filters that are used for realization of CMT and SMT systems. Thus, here, also, we follow the continuous-time approach of [19, 38].

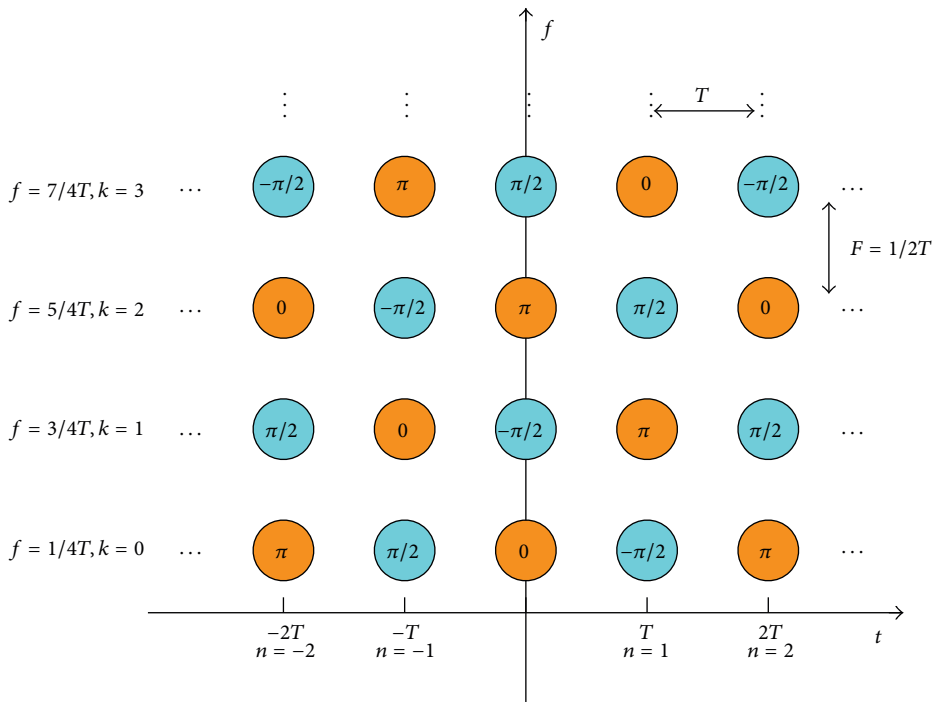

Figure 1: The CMT time-frequency phase-space lattice.

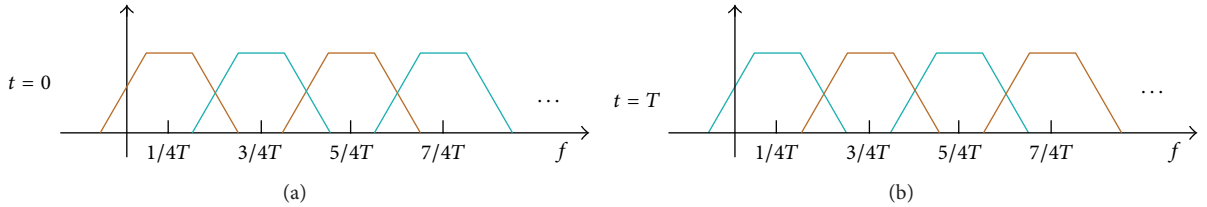

Figure 2: Magnitude responses of the CMT pulse-shaping filters at various subcarriers and time instants $t = 0$ and $t = T$.

Moreover, to give a complement presentation to those of [19, 38], an attempt is made to discuss the underlying theory mostly through the *time-frequency phase-space*, with minimum involvement in mathematical details. It is believed that this presentation also provides a new intuition into the relationship between SMT and CMT. Interested readers who wish to see the mathematical details are referred to [20, 38].

3.1. CMT. In CMT, data symbols are from a pulse amplitude modulated (PAM) alphabet and, hence, are real-valued. To establish a transmission with the maximum bandwidth efficiency, PAM symbols are distributed in a time-frequency phase-space lattice with a density of two symbols per unit area. This is equivalent to one complex symbol per unit area. Moreover, because of the reasons that are explained below a 90-degree phase shift is introduced to the respective carriers among the adjacent symbols. These concepts are presented in Figure 1. Vestigial side-band (VSB) modulation is applied to cope with the carrier spacing $F = 1/2T$. The pulse-shape used for this purpose at the transmitter as well as for matched filtering at the receiver is a square-root Nyquist waveform, $p(t)$, which has been designed such that $q(t) = p(t) \star p(-t)$ is a Nyquist pulse with regular zero crossings at $2T$ time intervals. Also, $p(t)$, by design, is a real-valued function of time and $p(t) = p(-t)$. These properties of $p(t)$, as demonstrated below, are instrumental for correct functionality of CMT.

Figure 2 presents a set of magnitude responses of the modulated versions of the pulse-shape $p(t)$ for the data symbols transmitted at $t = 0$ and $t = T$. The colors used for the plots follow those in Figure 1 to reflect the respective phase shifts.

Let $n = \ldots, -2, -1, 0, 1, 2, \ldots$, denote symbol time index, let $k = 0, 1, 2, \ldots$, denote symbol frequency index, let $s_k[n]$ denote the (n, k) data symbol in the time-frequency lattice, and let $\theta_k[n] = (k - n)(\pi/2)$ be the phase shift that is added to the carrier of $s_k[n]$. Accordingly, a CMT waveform that is constructed based on the pulse-shape/prototype filter $p(t)$ is expressed as

$$x(t) = \sum_n \sum_k s_k[n]\, a_{n,k}(t), \tag{1}$$

where

$$a_{n,k}(t) = e^{j\theta_k[n]}\, p_{n,k}(t),$$
$$p_{n,k}(t) = p(t - nT)\, e^{j((2k+1)\pi/2T)t}. \tag{2}$$

The synthesis of $x(t)$ according to (1) has the following interpretations. The terms $a_{n,k}(t)$ may be thought as a set of basis functions that are used to modulate the data symbols $s_k[n]$. The data symbols $s_k[n]$ can be extracted from $x(t)$ straightforwardly if $a_{n,k}(t)$ are a set of orthogonal basis functions. The orthogonality for a pair of functions $v_1(t)$ and $v_2(t)$, in general, is defined as

$$\left\langle v_1(t), v_2(t)\right\rangle = \int_{-\infty}^{\infty} v_1(t)\, v_2^*(t)\, dt = 0. \tag{3}$$

For the case of interest here, where the data symbols $s_k[n]$ are real-valued, the orthogonality definition (3) can be replaced by the more relaxed definition:

$$\left\langle v_1(t), v_2(t)\right\rangle_R = \Re\left\{\int_{-\infty}^{\infty} v_1(t)\, v_2^*(t)\, dt\right\} = 0, \tag{4}$$

where $\Re\{\cdot\}$ indicates the real part. Definition (4) is referred to as *real orthogonality*.

It is not difficult to show that

$$\left\langle a_{n,k}(t), a_{m,l}(t)\right\rangle_R = \begin{cases} 1, & n = m,\ k = l \\ 0, & \text{otherwise} \end{cases} \tag{5}$$

and, hence, for any pair of n and k,

$$s_k[n] = \left\langle x(t), a_{n,k}(t)\right\rangle_R. \tag{6}$$

To develop an in-depth understanding of the CMT signaling, it is instructive to explore a detailed derivation of (5). To this end, we begin with the definition

$$\begin{aligned} &\left\langle a_{n,k}(t), a_{m,l}(t)\right\rangle_R \\ &\quad = \Re\left\{\int_{-\infty}^{\infty} e^{j\theta_k[n]}\, p_{n,k}(t)\, e^{-j\theta_l[m]}\, p_{m,l}^*(t)\, dt\right\} \end{aligned} \tag{7}$$

and note that this can be rearranged as

$$\begin{aligned} &\left\langle a_{n,k}(t), a_{m,l}(t)\right\rangle_R \\ &\quad = \Re\left\{\int_{-\infty}^{\infty} e^{j(m-n+k-l)(\pi/2)}\, p(t-nT) \right. \\ &\qquad \left. \times\, p(t-mT)\, e^{j((k-l)\pi/T)t} dt\right\}. \end{aligned} \tag{8}$$

When $m = n$ and $k = l$, after a change of variable t to $t + nT$, (8) reduces to

$$\begin{aligned} \left\langle a_{n,k}(t), a_{n,k}(t)\right\rangle_R &= \int_{-\infty}^{\infty} p^2(t)\, dt \\ &= 1, \end{aligned} \tag{9}$$

where the second equality follows from the fact that $p(t)$ is a real-valued square-root Nyquist pulse and $p(t) = p(-t)$.

When $k = l$, $m \neq n$, and $m - n = 2r$, where r is an integer,

$$\begin{aligned} \left\langle a_{n,k}(t), a_{n,k}(t)\right\rangle_R &= (-1)^r \int_{-\infty}^{\infty} p(t-nT)\, p(t-mT)\, dt \\ &= 0, \end{aligned} \tag{10}$$

where the second equality follows since $p(t)$ is a square-root Nyquist pulse, designed for a symbol spacing $2T$. On the other hand, when $k = l$, but $m - n = 2r + 1$,

$$\begin{aligned} &\left\langle a_{n,k}(t), a_{n,k}(t)\right\rangle_R \\ &\quad = \Re\left\{j(-1)^r \int_{-\infty}^{\infty} p(t-nT)\, p(t-mT)\, dt\right\} \\ &\quad = 0. \end{aligned} \tag{11}$$

Next, consider the case where $k - l = 1$ and $m - n = 2r$. In that case, one finds that

$$\begin{aligned} &\left\langle a_{n,k}(t), a_{m,l}(t)\right\rangle_R \\ &\quad = \Re\left\{j(-1)^r \int_{-\infty}^{\infty} p(t-nT)\, p(t-mT)\, e^{j(\pi/T)t} dt\right\} \\ &\quad = -(-1)^r \int_{-\infty}^{\infty} p(t-nT)\, p(t-mT) \sin\left(\frac{\pi}{T}t\right) dt \\ &\quad = 0, \end{aligned} \tag{12}$$

where the last identity follows, by applying the change of variable $t \rightarrow t + ((m+n)/2)T$ and noting that the expression under the integral will reduce to an odd function of t. Following similar procedures, it can be shown that the real orthogonality $\langle a_{n,k}(t), a_{m,l}(t)\rangle_R = 0$ also holds, when $k - l = 1$ and $m - n$ is an odd integer, and when $k - l = -1$ and $m - n$ is either an even or odd integer. Finally, for the cases where $|k - l| > 1$, the real orthogonality $\langle a_{n,k}(t), a_{m,l}(t)\rangle_R = 0$ is trivially confirmed by noting that the underlying basis functions correspond to filters that have no overlapping bands. The stop-band quality of the frequency response of the prototype filter $p(t)$ determines the accuracy of the equality $\langle a_{n,k}(t), a_{m,l}(t)\rangle_R = 0$ when $|k - l| > 1$.

It is also worth noting that some of the recent derivations of FBMC that are presented in discrete-time design the respective prototype filter $p[n]$ such that the respective real orthogonality is perfectly satisfied for the cases where $|k - l| > 1$ as well, for example, [56]. However, one may realize that, in practice, the presence of channel destroys the orthogonality of the basis functions. The orthogonality of the basis functions is commonly recovered at the receiver using per subcarrier equalizers; see Section 6, below. Such equalizers, unfortunately, will not be able to recover the orthogonality of basis functions that belong to nonadjacent subcarriers. Hence, the design of a $p[n]$ that satisfies the real orthogonality for $|k - l| > 1$ may be a waste.

To summarize, the above derivations revealed that the following settings of the CMT parameters lead to the real orthogonality of the basis functions $a_{n,k}(t)$ and allow symbol placement in the time-frequency lattice at the maximum density of two real symbols per unit area.

(1) The symbol spacing T along the time axis should be matched with the subcarrier spacing $F = 1/2T$ along the frequency axis.

(2) The pulse-shape/prototype filter $p(t)$ must be a real-valued square-root Nyquist filter for a symbol spacing

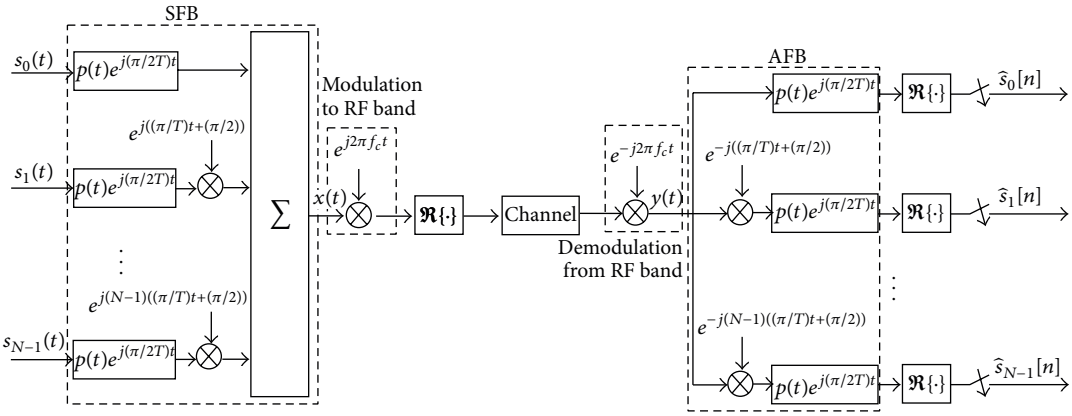

Figure 3: CMT transmitter and receiver blocks.

$2T$. It should be also a linear phase; hence, when viewed as a zero phase filter, it satisfies the condition $p(t) = p(-t)$. The latter is not a necessary condition but is satisfied in most of the designs; see [38] for a more relaxed condition.

(3) The above constraints are applied to assure orthogonality of the basis functions that are within the same subcarrier or adjacent subcarriers only. The orthogonality of basis functions that belong to the nonadjacent subcarriers is guaranteed by virtue of the fact that they correspond to filters with nonoverlapping bands. A more advanced design presented in Section 4.2 allows overlapping of the nonadjacent bands and yet satisfies the orthogonality condition.

(4) The phase shifts indicated in Figure 1 can be modified to other choices, as long as a phase difference $\pm\pi/2$ is preserved between each pair of adjacent points in the lattice.

(5) Although in CMT the position of the lattice points is fixed, these points can be moved in the time-frequency plane as long as their relative position and phase differences remain unchanged. We use this point below to arrive at the SMT waveform by applying a simple modification to the CMT waveform (1).

The above equations may be combined to arrive at the CMT transmitter and receiver structures that are presented in Figure 3. As shown a synthesis filter bank (SFB) is used to construct the transmit signal, and the received signal is passed through an analysis filter bank (AFB) to separate the data streams of different subcarrier bands. Here, it is assumed that there are N subcarrier streams and the data stream of the kth subcarrier at the input to the SFB is represented by the impulse train:

$$s_k(t) = \sum_n s_k[n]\,\delta(t - nT). \tag{13}$$

It is also worth noting that, in practice, the analyzed signals at the output of the AFB should be equalized. Here, to keep the presentation simple, we have not included the equalizers. Equalizer details are presented in Section 6.

3.2. SMT. SMT may be thought of as an alternative to CMT. Its time-frequency phase-space lattice is obtained from that of CMT (Figure 1) through a frequency shift of the lattice points down by $1/4T$, scaling the time axis by a factor $1/2$ and hence the frequency axis by a factor 2. Moreover, to remain consistent with the past literature of SMT (equivalently, OQAM-OFDM), some adjustments to the carrier phases of the lattice points have been made. This leads to the time-frequency phase-space lattice that is presented in Figure 4. The magnitude responses of the SMT pulse-shaping filters at various subcarriers and time instants $t = 0$ and $t = T/2$ are presented in Figure 5. Note that here the PAM symbols are spaced by $T/2$ and subcarriers are spaced by $1/T$. In SMT, each pair of adjacent symbols along time in each subcarrier is treated as real and imaginary parts of a QAM symbol. This leads to the transmitter and receiver structures that are presented as in Figure 6. Here, each data symbol $s_k[n]$ belongs to a QAM constellation and, thus, may be written in terms of its in-phase and quadrature components as $s_k[n] = s_k^I[n] + js_k^Q[n]$. Accordingly, the inputs to the SFB in Figure 6 are

$$\begin{aligned} s_k^I(t) &= \sum_n s_k^I[n]\,\delta(t - nT), \\ s_k^Q(t) &= \sum_n s_k^Q[n]\,\delta(t - nT). \end{aligned} \tag{14}$$

3.3. FMT. FMT waveforms are synthesized following the conventional method of frequency division multiplexing (FDM). The subcarrier channels have no overlap, and thus ICI is resolved through use of well-designed filters with high stopband attenuation. ISI may be compensated for by adopting the conventional method of square-root Nyquist filtering that is used in single-carrier communications. For doubly dispersive channels, we have adopted a more advanced design [57] that compensates for both ICI and ISI through an effective method which is presented in Section 4.2.

For comparison with the CMT and SMT structures in Figures 3 and 6, respectively, and also as a basis for further

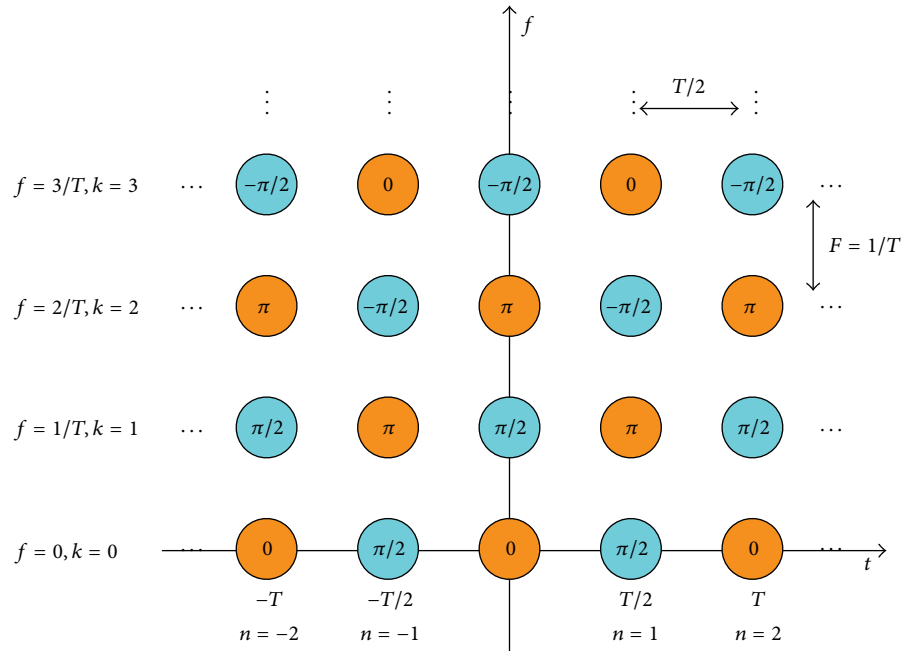

Figure 4: The SMT time-frequency phase-space lattice.

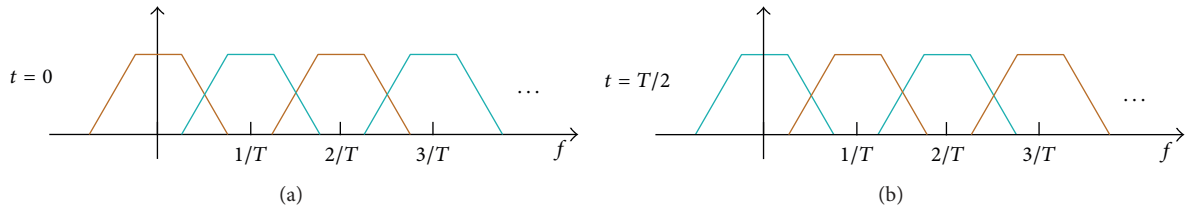

Figure 5: Magnitude responses of the SMT pulse-shaping filters at various subcarriers and time instants $t = 0$ and $t = T/2$.

development in later parts of this paper, Figure 7 presents the structures of transmitter and receiver blocks in an FMT communication system. Also, the magnitude responses of the FMT pulse-shaping filters at various subcarriers are presented in Figure 8. Note that here the subcarrier spacing is equal to $(1 + \alpha)/T$, where α is the roll-off factor of the pulse-shaping/prototype filter. Accordingly, FMT has a symbol density of $1/(1+\alpha)$ complex symbols per unit area in the time-frequency plane. Hence, FMT is less bandwidth efficient than CMT and SMT.

4. Prototype Filter Design

The results of the previous section suggest that linear phase square-root Nyquist filters that have been widely used for single carrier data transmission are the most trivial choice for prototype filter in FBMC systems. This indeed remains an accurate statement as long as the underlying channel is time-invariant or varies slowly. However, in cases where the channel is fast varying, a more general class of square-root Nyquist filters that satisfy the Nyquist condition both along the time and frequency axis should be adopted. In this section, we first review couple of classical Nyquist designs developed by us [58] and others [59], and then discuss an example of more advanced designs that also have been developed in our research group [57] and is more appropriate for time-varying channels.

4.1. Prototype Filters for Time-Invariant Channels. The classical prototype filter for FBMC systems that was suggested in [39, 40] was the square-root raised-cosine (SRRC) filter. More specifically, both [39, 40] suggested using a SRRC filter with the roll-off factor $\alpha = 1$. In practice, where FBMC systems are implemented in discrete-time, SRRC response should be sampled and truncated. The truncation of the SRRC response may result in a filter with poor frequency response and, hence, makes SRRC a poor choice. Advancements in digital filters design have led to very effective methods for designing square-root Nyquist (SR-Nyquist) filters for any specified finite length. These designs, two of which are presented here, aim at balancing the stopband attenuation and the Nyquist property of the designs.

Martin [59] has proposed a design method whose goal is to satisfy the Nyquist criterion approximately while achieving good attenuation in the stopband. A nice property of this method is that when the number of samples per symbol

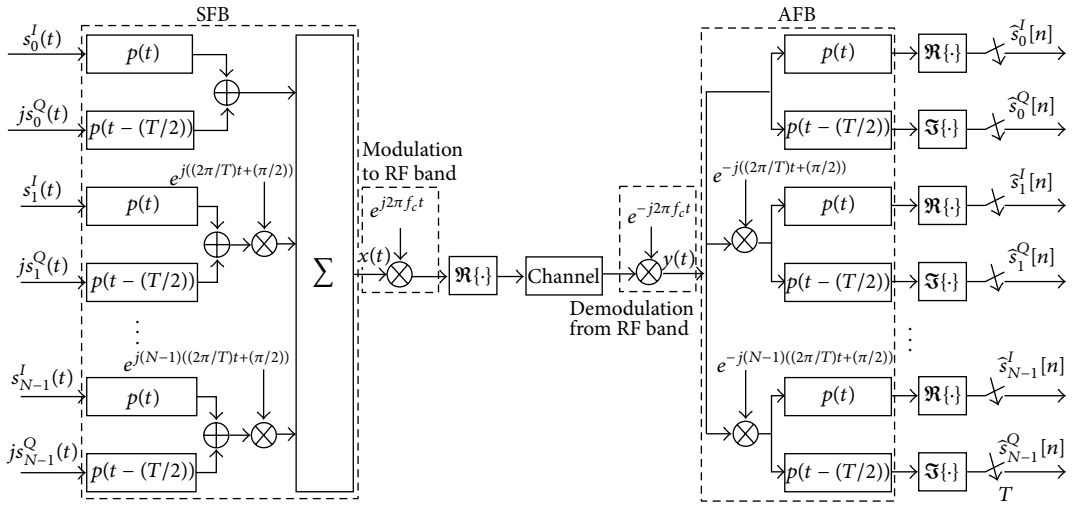

Figure 6: SMT transmitter and receiver blocks.

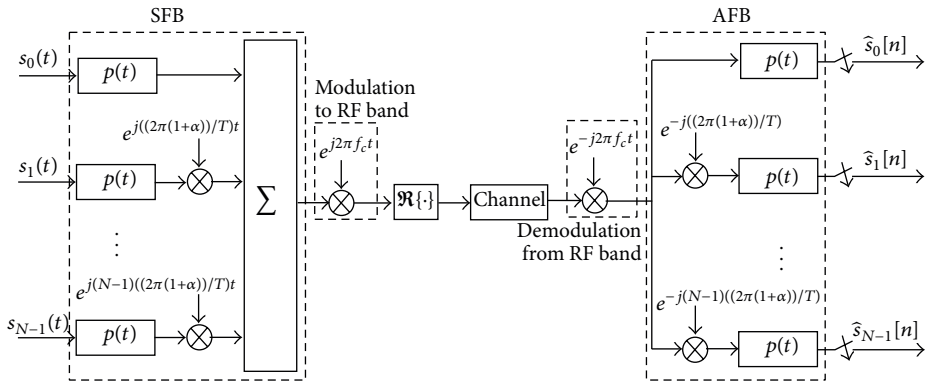

Figure 7: FMT transmitter and receiver blocks.

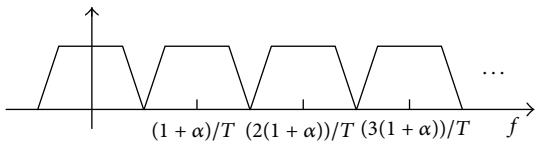

Figure 8: Magnitude responses of an FMT pulse-shaping filter at various subcarriers.

interval is N and the filter length is $\beta N + 1$, where β is an integer greater than 1, there are only β parameters that need to be found for the optimization of the design. More specifically, the prototype filter is constructed as

$$p[n] = \begin{cases} \dfrac{1}{\beta N+1}\left(k_0 + 2\displaystyle\sum_{l=1}^{\beta-1} k_l \cos\left(\dfrac{2\pi l n}{\beta N+1}\right)\right), & 0 \le n \le \beta N \\ 0, & \text{otherwise,} \end{cases} \tag{15}$$

where the coefficients k_0 through $k_{\beta-1}$ are to be optimized. The optimum choices of the coefficients k_0 through $k_{\beta-1}$, for different values of β, are tabulated in [59] and, also, in [60]. Beside being a simple and effective method, it is important to note that Martin's design for $\beta = 4$ has been adopted by the PHYDYAS project [21].

More recently, we have developed an algorithm for designing SR-Nyquist filters that can balance between the accuracy of the Nyquist constraints and the filter stopband attenuation [58]. To select the samples of the zero-phase impulse response $p[n] = p[-n]$ of the SR-Nyquist filter, this algorithm defines

$$q[n] = p[n] \star p[-n] \tag{16}$$

and minimizes the cost function

$$\xi = (q[0]-1)^2 + \sum_{m=1}^{K/2} q^2[mN] + \gamma \int_{(1+\alpha)/2N}^{1-((1+\alpha)/2N)} |P(f)|^2 \, df \tag{17}$$

with respect to the elements $p[n]$. The first two terms on the right-hand side of (17) are to enforce Nyquist property on $q[n]$, and the third term is included to minimize the stopband response of $p[n]$. Also, the length of $p[n]$ is assumed to be

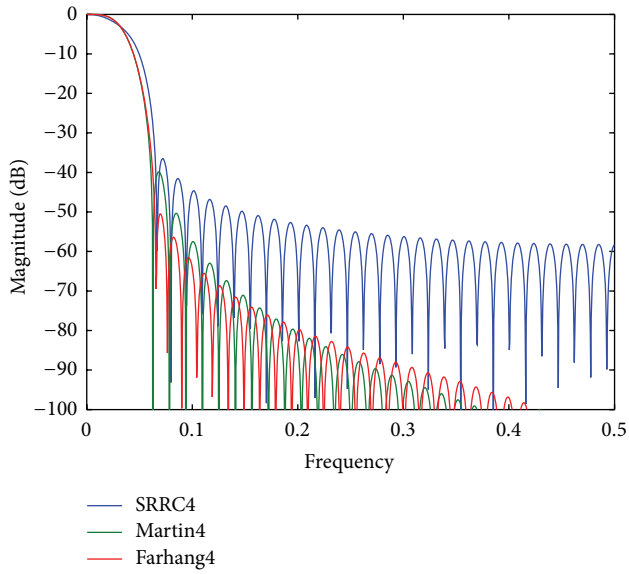

Figure 9: Magnitude responses of a sampled and truncated SRRC filter and two discrete-time designed SR-Nyquist filters.

equal to $\beta N + 1$. One may note that since ξ is a forth-order function of the parameters $p[n]$, it is a multimodal function and hence its minimization may not be straightforward. However, fortunately, if $p[n]$ could be initialized near its optimum choice, an iterative solution may be applied to search for the local minimum of ξ. The search algorithm proposed in [58] follows a similar procedure to the one originally suggested in [61].

Figure 9 presents the magnitude responses of three designs based on (i) a sampled and truncated version of the impulse response of a SRRC filter: SRRC4; (ii) a SR-Nyquist design obtained following [59]: Martin4; and (iii) a SR-Nyquist design obtained following [58]: Farhang4. All designs are based on the roll-off factor $\alpha = 1$ and are for an FBMC system with $N = 16$ subcarriers, and the suffix 4 on the names indicates that, for all designs, $\beta = 4$; that is, the designed filters have a length $\beta N + 1 = 4 \times 16 + 1 = 65$. In addition, for Farhang4, the parameter γ (defined in [58]) is set equal to 0.1.

As seen, and one would expect, SRRC design performs significantly inferior to both of the SR-Nyquist designs. From the two SR-Nyquist designs, the one based on [58] achieves a higher attenuation in the first few sidelobes of its stopband than the design based on [59]. The first sidelobe of the former design is 10 dB lower. Also, a study of the time domain responses of the designs reveals that none of them satisfies the Nyquist property perfectly. Hence, all are near Nyquist designs. However, the design of [59] is the closest to Nyquist, followed by the design delivered by [58] and, then, the SRRC design. Nevertheless, all the three designs are very close to Nyquist; hence, the choice of one against the others may be dominantly determined by its superior magnitude response.

4.2. Prototype Filters for Time-Varying Channels. When a channel is subject to dispersion both in time (due to multipath effects) and in frequency (due to variation of the channel in time), we say the channel is *doubly dispersive*. We also note that while the dominant effect of time dispersion in a channel is ISI, the dominant effect of frequency dispersion is ICI. Hence, in order to design prototype filters that address both time and frequency dispersions, it has been argued [44] that one should choose a pulse-shape $p(t)$ with similar behavior along time and frequency. In particular, if $p(t)$ is selected to be a SR-Nyquist along the time axis, it should be also made sure that $P(f)$ is a SR-Nyquist along the frequency axis. To this end, the pulse-shape, $p(t)$, with the following property may be adopted:

$$P(f) = p(\eta f), \quad \text{for a constant scaling factor } \eta, \tag{18}$$

that is, a function that has the same form in both time and frequency domains.

The parameter η in (18) is related to the symbol spacing in time, T, and frequency, F, and is given by

$$\eta = \frac{T}{F}. \tag{19}$$

Also, as one may understand intuitively, T and F are, respectively, chosen proportional to time dispersion, $\Delta\tau$, and frequency dispersion, $\Delta\nu$, of the channel; that is, $T/F = \Delta\tau/\Delta\nu$. Hence, the following identity also holds:

$$\eta = \frac{\Delta\tau}{\Delta\nu}. \tag{20}$$

The definitions for $\Delta\tau$ and $\Delta\nu$ are usually vague. The time dispersion $\Delta\tau$ may be thought of as a coarse estimate of the duration of the channel impulse response, equivalently the span of the multipaths of the channel. Similarly, the frequency dispersion $\Delta\nu$ may be thought of as a coarse estimate of the span of Doppler spread of the channel.

The design of the prototype filter for time-varying channels is closely tied to the ambiguity function [62–64]:

$$A_p(\tau, \nu) = \int_{-\infty}^{\infty} p\left(t + \frac{\tau}{2}\right) p^*\left(t - \frac{\tau}{2}\right) e^{-j2\pi\nu t} dt, \tag{21}$$

where τ is a time delay and ν is a frequency shift.

Let $p(t)$ be a prototype filter and let $p_{n,k}(t)$ be a time frequency translated version of it which is defined as

$$p_{n,k}(t) = p(t - nT) e^{j2\pi kFt}. \tag{22}$$

We note that

$$\begin{aligned} &\langle p_{m,k}(t), p_{n,l}(t) \rangle \\ &\quad = \int_{-\infty}^{\infty} p(t - mT) e^{j2\pi kFt} p(t - nT) e^{-j2\pi lFt} dt \\ &\quad \propto A_p((n - m)T, (l - k)F), \end{aligned} \tag{23}$$

where $\propto$ indicates proportionate to. The proportionate factor is a phase shift due to the delays of mT and nT whose value is irrelevant to our discussion here. Using (23), one may note that $p_{n,k}(t)$ of (22), for all choices of n and k, will form a set of

complex-valued orthogonal basis functions, if $p(t)$ is chosen such that

$$A_p(nT, lF) = \begin{cases} 1, & n = l = 0 \\ 0, & \text{otherwise.} \end{cases} \quad (24)$$

We note that the case where $\nu = 0$ corresponds to the familiar (time) correlation function:

$$A_p(\tau, 0) = \int_{-\infty}^{\infty} p\left(t + \frac{\tau}{2}\right) p\left(t - \frac{\tau}{2}\right) dt \quad (25)$$

which reduces to the Nyquist constraints:

$$A_p(nT, 0) = \begin{cases} 1, & n = 0 \\ 0, & n \neq 0. \end{cases} \quad (26)$$

Also, one may note that the integral on the right-hand side of (25) is equal to the convolution of $p(t)$ and its matched pair $p(-t)$, evaluated at time $t = \tau$. Thus, $A_p(t, 0) = p(t) \star p(-t)$ and, hence, (26) implies that $p(t)$ is a SR-Nyquist pulse. Moreover, the ambiguity function $A_p(\tau, \nu)$ may be thought of as a generalization of the correlation function $A_p(\tau, 0)$ where correlation is found between $p(t)$ and its modulated version at the frequency $f = \nu$. Accordingly, we refer to the set of constraints (24) as the *generalized Nyquist constraints*.

Another key point that one should consider in the selection of $p(t)$, for time-varying channels, is minimization of its duration. Le Floch et al. [44] have noted that to maximize the density of the basis functions $p_{n,k}(t)$ in the time-frequency space and, hence, maximize the bandwidth efficiency of the transmission, one should choose a $p(t)$ that has maximum compactness in the time-frequency space. Maximum compactness, on the other hand, is quantified by the product $\sigma_t \sigma_f$, where σ_t^2 and σ_f^2 are, respectively, the second-order moments of the functions $p(t)$ and $P(f)$. Moreover, the Heisenberg-Gabor uncertainty principle states that [65]

$$\sigma_t \sigma_f \geq \frac{1}{4\pi}, \quad (27)$$

where the equality holds only when $p(t)$ is the Gaussian pulse $g(t) = e^{-\pi t^2}$. Also, the Gaussian pulse $g(t)$ has the interesting property that $G(f) = g(f)$; that is, it satisfies the desirable property (18), with $\eta = 1$. However, $p(t) = g(t)$ does not satisfy the orthogonality conditions (24).

Attempts to design filters that satisfy the orthogonality conditions (24) and at the same time approach the Heisenberg-Gabor uncertainty lower bound (27) as close as possible have been made and design methods have been developed [44, 66]. The design presented in [44] is called *isotropic* orthogonal transform algorithm (IOTA) filter. IOTA design/algorithm was first introduced in a patent by Alard [67]. The designs proposed in [66], on the other hand, are referred to as *Hermite pulses*, reflecting the fact that their construction is based on a linear combination of a set of Hermite functions. In the rest of this section, we limit our emphasis to the design of Hermite pulses and emphasize the flexibilities that these designs provide in adopting to doubly dispersive channels. More details on this topic can be found in [57] (also, see [68, 69]). Discussion on IOTA design can be found in [19, 20, 44, 70].

The design procedure proposed by Haas and Belfiore [66] constructs an isotropic filter according to the equation:

$$p(t) = \sum_{k=0}^{L} \alpha_k h_{4k}(t), \quad (28)$$

where $\{h_n(t)\}$ is the set of Hermite functions defined as

$$h_n(t) = \frac{1}{(2\pi)^{n/2}} e^{\pi t^2} \frac{d^n}{dt^n} e^{-2\pi t^2}. \quad (29)$$

Note that $h_0(t) = g(t)$ and, thus, it is an isotropic function with parameter $\eta = 1$. Moreover, it can be shown that the set of functions $h_n(t)$ for $n = 4k$, $k = 1, 2, \ldots$, are also isotropic, with the same parameter. This implies that the construction (28) for any set of coefficients α_k leads to an isotropic function. In [66], the coefficients α_k have been calculated to construct a filter $p(t)$ that satisfies the set of constraints (24), for parameters $T = F = \sqrt{2}$.

Haas and Belfiore's design [66] allows transmission of QAM symbols with a density of $1/TF = 0.5$ symbol per unit area in the time-frequency space. This design of $p(t)$ may also be used as the prototype filter in a CMT or SMT structure to increase the density to 2 PAM symbols per unit area, equivalent to one QAM symbol per unit area. Alternatively, one can aim for a design with larger density than 0.5 and stay with transmitting QAM symbols. Examples of both designs are presented later. In the rest of this section, we follow the approach of [57] to present a broad class of Hermite filter designs that includes the design presented in [66] as a special case.

The basic equations for the design of Hermite pulses are obtained by substituting (28) in (21). This gives

$$\begin{aligned} A_p(\tau, \nu) &= \int_{-\infty}^{\infty} \sum_{n=0}^{L} \sum_{l=0}^{L} \alpha_n \alpha_l h_{4n}\left(t + \frac{\tau}{2}\right) h_{4l}\left(t - \frac{\tau}{2}\right) e^{-j2\pi\nu t} dt \\ &= \sum_{n=0}^{L} \sum_{l=0}^{L} \alpha_n \alpha_l A_{n,l}(\tau, \nu), \end{aligned} \quad (30)$$

where

$$A_{n,l}(\tau, \nu) = \int_{-\infty}^{\infty} h_{4n}\left(t + \frac{\tau}{2}\right) h_{4l}\left(t - \frac{\tau}{2}\right) e^{-j2\pi\nu t} dt. \quad (31)$$

Defining

$$\boldsymbol{\alpha} = \begin{bmatrix} \alpha_0 & \alpha_1 & \cdots & \alpha_L \end{bmatrix}^T,$$

$$\mathbf{A}(\tau, \nu) = \begin{bmatrix} A_{0,0}(\tau, \nu) & A_{0,1}(\tau, \nu) & \cdots & A_{0,L}(\tau, \nu) \\ A_{1,0}(\tau, \nu) & A_{1,1}(\tau, \nu) & \cdots & A_{1,L}(\tau, \nu) \\ \vdots & \vdots & \ddots & \vdots \\ A_{L,0}(\tau, \nu) & A_{L,1}(\tau, \nu) & \cdots & A_{L,L}(\tau, \nu) \end{bmatrix}, \quad (32)$$

(30) may be rearranged as

$$A_p(\tau,\nu) = \boldsymbol{\alpha}^T \mathbf{A}(\tau,\nu)\,\boldsymbol{\alpha}. \tag{33}$$

(1) Haas and Belfiore Design. In [66], it was proposed that the coefficients α_0 through α_L can be determined by substituting (33) into (24) for $(n,l) = (0,0)$ and L other significant choices of (n,l) and solving the resulting system of equations. It was, numerically, demonstrated that this leads to very good designs. To further clarify this procedure and pave the way for additional developments in the sequel, we discuss the method of [66] in the context of a specific design. Figure 10 presents the grid of all choices of (n,l). Here, it is assumed that the constraints (24) are applied at the origin and the 12 nearest grid points to it. In this figure, three different sets of grid points are identified.

(1) The significant points are the ones at which the constraints (24) should be imposed. There are four such points and these are indicated by red disks.

(2) Once the desired constraints are imposed at the significant points defined in (1), it follows from the even symmetry and isotropic property of $p(t)$ that the same constraints will automatically be imposed at the rest of the points indicated by green disks.

(3) The remaining grid points, indicated by white disks, will satisfy the constraints (24), within a good approximation, since the designed pulse $p(t)$ decays exponentially/fast as $|t|$ increases.

We note that to satisfy the constraints (24) at the origin and the 12 nearest grid points to it, it is sufficient to apply constraints to only 3 of the latter points. A unique design is thus obtained if the design is made based on $h_0(t), h_4(t), h_8(t)$, and $h_{12}(t)$, that is, the choice of $L = 3$ in (30) through (33).

It should be also noted that since, here, the designed filter is isotropic, with the parameter $\eta = 1$, the identity $T = F$ should hold. Hence, given a desired density $D = 1/TF$, the design must be for the parameters $T = F = 1/\sqrt{D}$. Once $p(t)$ is obtained based on these parameters, applying a time scaling factor, one can set T to any desired value. This will set F equal to $1/TD$.

(2) Hexagonal Lattice. The spread of data symbols in Figure 10 and other lattice grids that have been presented in this paper, so far, follows an orientation that is referred to as *rectangular* lattice. In [71], it is noted that better designs may be obtained by adopting the *hexagonal* orientation. The reason behind this improvement in performance follows the fact that the hexagonal orientation allows maximum separation of points for a given symbol density. Interested readers are referred to the detailed discussions in [19, 20, 71].

To design prototype filters for an orientation that follows the hexagonal lattice, we choose the constrained points according to those depicted in Figure 11. It should be noted that we set $T = 2F$ and for this choice it is sufficient to enforce design constraints at the points indicated by red disks. As in the case of rectangular lattice, once the constraints are applied to these points, similar constraints will be automatically imposed to the points indicated by green disks, following the symmetric and isotropic property of the designs. Moreover, as in the case of rectangular lattice, by design, the remaining grid points, indicated by white disks, will satisfy the constraints (24), within a good approximation. Finally, a time scaling can be applied to $p(t)$ to set T, and accordingly F, to any desired value.

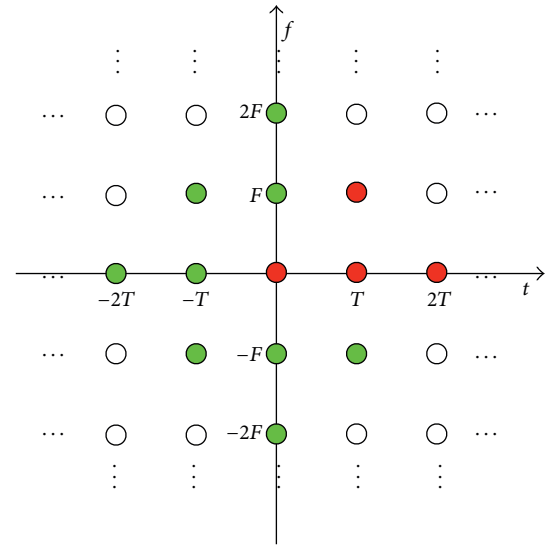

Figure 10: Grid of (n,k) points at which the constraints (24) should be imposed. The red disks indicate the points at which the constraints (24) are imposed. The green disks follow the red ones, thanks to symmetric and isotropic property of the design. The rest of the points (white disks) satisfy the constraints within a good approximation, since the construction is based on exponentially decaying pulses as $|t|$ increases.

(3) Robust Design. Building on the above findings, we noted that, in a practical design, the time and frequency dispersion introduced by a channel smear the null points of the ambiguity function $A_p(\tau,\nu)$ [57, 68, 69]. Hence, as a result of the channel dispersion, the nulls will convert to shallow nulls. It is, thus, argued that instead of designing $p(t)$ to introduce perfect nulls in $A_p(\tau,\nu)$, a more robust design is obtained by aiming for a design that results in deep (but imperfect) null areas around the grid points (nT, kF). To this end, a robust Hermite pulse is designed by minimizing the cost function:

$$\begin{aligned}\zeta = {} & \gamma_0 \int_{\mathscr{A}_0} \left|\boldsymbol{\alpha}^T \mathbf{A}(\tau,\nu)\boldsymbol{\alpha} - 1\right|^2 d\tau\, d\nu \\ & + \sum_{k=1}^{L} \gamma_k \int_{\mathscr{A}_k} \left|\boldsymbol{\alpha}^T \mathbf{A}(\tau,\nu)\boldsymbol{\alpha}\right|^2 d\tau\, d\nu,\end{aligned} \tag{34}$$

where $\mathscr{A}_0$ is an area around the origin and $\mathscr{A}_1$ through $\mathscr{A}_L$ are the null areas that are aimed for.

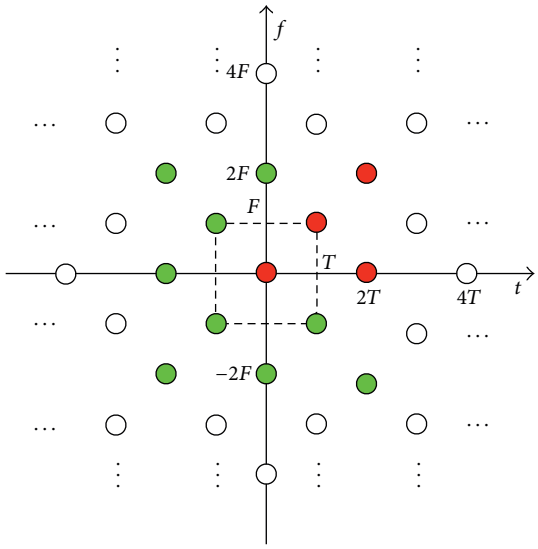

Figure 11: Grid of (n, k) points for hexagonal orientation. The red disks indicate the points at which the constraints (24) are imposed. The green disks follow the red ones, thanks to symmetric and isotropic property of the design. The rest of the points (white disks) satisfy the constraints within a good approximation, since the construction is based on exponentially decaying pulses as $|t|$ increases.

To develop a numerical method for the minimization of ζ, the ambiguity function is sampled along the time axis τ and the frequency axis ν. This converts (34) to

$$\zeta = T_s F_s \left(\sum_{k=0}^{L} \sum_{(mT_s, nF_s) \in \mathcal{A}_k} \gamma_k \left| \boldsymbol{\alpha}^T \mathbf{A}(mT_s, nF_s) \boldsymbol{\alpha} - u_k \right|^2 \right), \quad (35)$$

where T_s and F_s are the sampling periods along the time axis and frequency axis, respectively, and

$$u_k = \begin{cases} 1, & k = 0 \\ 0, & k \neq 0. \end{cases} \quad (36)$$

Removing the third term on the right-hand side of (17), one may realize that the cost functions ξ and ζ are similar. Both are fourth-order functions of the parameters that we seek to optimize. Hence, the iterative method developed in [58] can be readily adopted here as well. For this purpose, as in [58], an initial guess for the elements of the parameter vector $\boldsymbol{\alpha}$ should be made. It has been noted in [57] that a proper initial choice for $\boldsymbol{\alpha}$ is the vector whose first element is 1 and the rest of its elements are 0. That is, one should start with the Gaussian pulse as a first guess and add the higher order Hermite functions in the subsequent iterations.

(4) Numerical Examples. To conclude this section, we present the results arising from a few designs of IOTA and Hermite prototype filters. Also, we compare the results with those of the SR-Nyquist design of [58].

Figure 12 presents the time domain and the magnitude of frequency domain responses of (i) an IOTA design [67], (ii) a Hermite design [66], and (iii) a SR-Nyquist design [58]. All designs have the same filter length of $4T$ and designed to serve a CMT/SMT system with a maximum of 16 subcarrier bands.

Considering the results presented in Figure 12, one may make the following observations.

(1) Both IOTA and Hermite designs have time-domain responses that are more compact than the time-domain response of the SR-Nyquist filter.

(2) In the frequency domain, on the other hand, the SR-Nyquist design gives a more compact response.

(3) The compact responses of IOTA and Hermite designs in time will make them less prone to distortion introduced by channel variation with time.

(4) The broader responses of IOTA and Hermite design in frequency, on the other hand, make them more prone to the channel frequency selectivity.

(5) Considering (3) and (4), a balance has to be made between the choice of the symbol interval, T, and the carrier spacing, F. Obviously, by applying a proper time scaling to the prototype filter $p(t)$, such balance can be made.

(6) When channel is time-invariant or varies slowly, the choice of SR-Nyquist results in the maximum immunity to the channel frequency selectivity.

The robust design approach that was presented above was first introduced in [69] and was further studied in [57, 68]. Here, to emphasize on the significance of this design approach, we present Figure 13 from [57]. This figure presents a set of results that compare the signal-to-interference ratio (SIR) of the robust isotropic designs (named FMT-dd: FMT for doubly dispersive channels) with OFDM and an FMT design according to the SR-Nyquist design of [58] (named FMC-c: conventional FMT). To measure SIR, the channel noise is set equal to zero. Three sets of results, corresponding to density values $D = 1/TF = 1/2, 2/3$, and $4/5$ are presented. The robust isotropic designs are obtained for a channel model in which dispersion in time and frequency is uniform in the intervals $(-\delta\tau/2, \delta\tau/2)$ and $(-\delta\nu/2, \delta\nu/2)$, respectively, and $\Delta\tau = 0.2T$ and $\Delta\nu = 0.2F$. The design for each density is fixed and its performance is examined for varying values of $\Delta\tau\Delta\nu$ in the range of 0 to 0.1. For FMT-c, the prototype filter is designed in each of the three cases with the aim of achieving a stopband attenuation of 60 dB or better. Also, following the basic principle of FMT-c, the roll-off factors of the prototype filters for density values $D = 1/2, 2/3$, and $4/5$ are set equal to 1, 0.5, and 0.25, respectively. For OFDM, the density $D = 1/TF$ is set by adjusting the ratio of cyclic prefix length, T_{CP}, over the length of FFT, T_{FFT}. In particular, we note that since in OFDM $F = 1/T_{\mathrm{FFT}}$ and $T = T_{\mathrm{CP}} + T_{\mathrm{FFT}}$, $D = T_{\mathrm{FFT}}/(T_{\mathrm{CP}} + T_{\mathrm{FFT}})$ and, thus, $T_{\mathrm{CP}}/T_{\mathrm{FFT}} = 1/D - 1$.

The results presented in Figure 13 clearly show the expected superior performance of the robust designs over OFDM and the conventional FMT design. The more detailed results presented in [57] for an underwater acoustic (UWA) communication further confirm these results in an at-sea experimental setting.

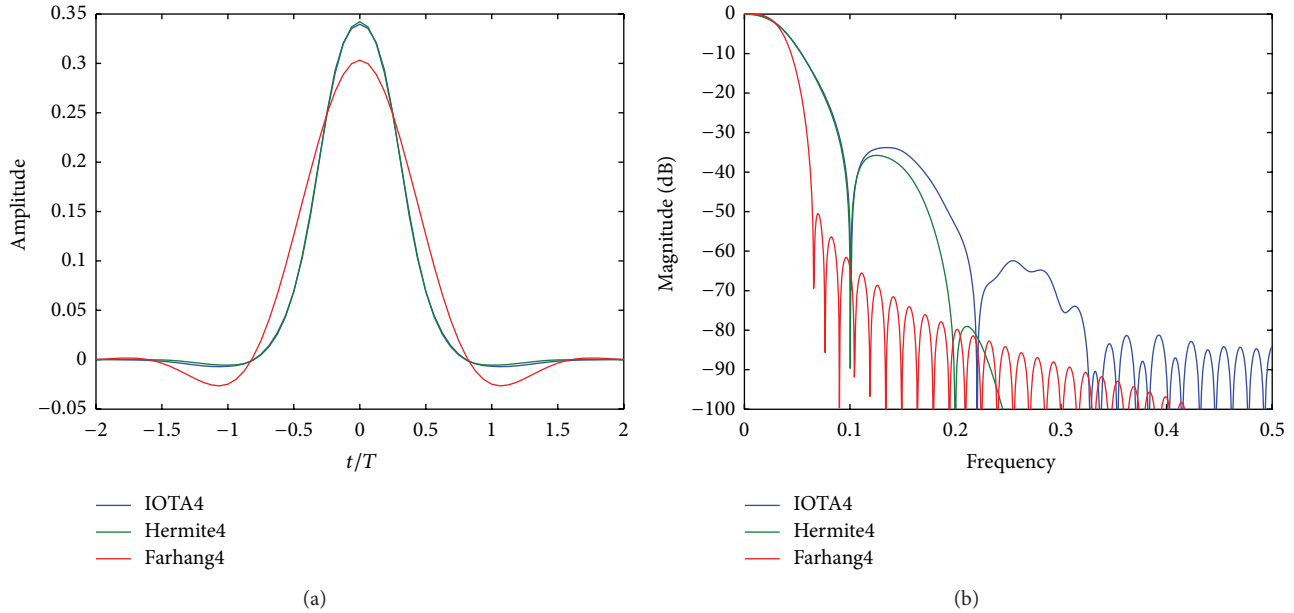

FIGURE 12: Responses of three designs of a prototype filter. (a) The time-domain responses. (b) The magnitude of the frequency-domain responses.

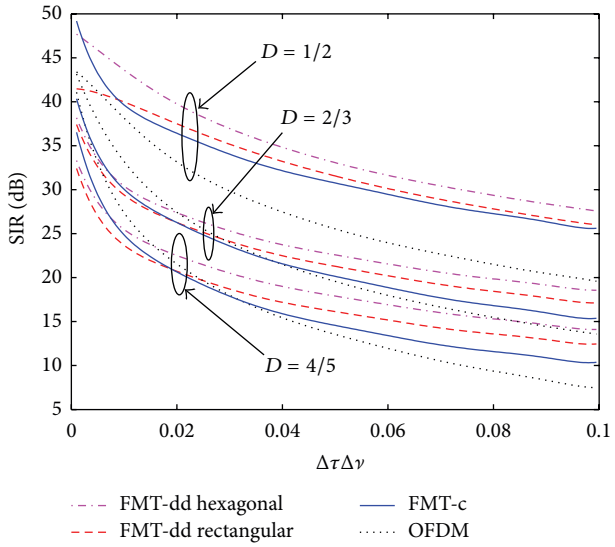

FIGURE 13: The impact of a doubly dispersive design and three designs of FMT. "FMT-c" is the case where a SR-Nyquist design is used. "FMT-dd" follows the robust design that was introduced above (the author obtained permission from IEEE to include this figure).

5. Polyphase Structures and Computational Complexity

Polyphase structures are commonly used to implement FBMC transmitter and receiver. Direct mimicking of the continuous-time structures of Figures 3 and 6 to implement CMT and SMT, respectively, may lead to structures whose complexity is not optimized. One polyphase structure per each set of real symbols, equivalent to two polyphase structures per each pair of real symbol sets, should be implemented. This section highlights the fact that the two polyphase structures at the transmitter side can be combined together and hence reduce the complexity to one half. At the receiver side, special attention has to be paid so that proper equalizers can be applied to the analyzed signal components. The presentation in this section, although results in structures with the same complexity to those already published, arrives at structures in more intuitive way and, thus, hopefully assists the reader to have a better grasp of the concepts.

Polyphase structures for FMT transmitter and receiver also need particular attention to take care of the fact that sampling rate changes in the AFB (at the transmitter side) and in the SFB (at the receiver side) is different from the size of IFFT/FFT block. A method that takes into account this change of sampling rate is presented in a later part of this section.

5.1. Polyphase Analysis and Synthesis Filter Banks. The basic polyphase SFB block that may be used to construct the SFB blocks in both CMT and SMT transmitter is presented in Figure 14. This block which is widely available and well developed in the literature, for example, see [49, 72], has the following characteristics.

(1) The inputs $\{s_k[n], k = 0, 1, \ldots, N-1\}$ are a set of data sequences with the nominal rate of unity.

(2) The SFB output has a rate of L or, equivalently, L times faster than the rate at the input.

(3) The synthesis is performed based on an IFFT of size $L > N$, with the inputs of index N and greater set equal to zero. This is to allocate some guard band between the generated baseband signal and its images

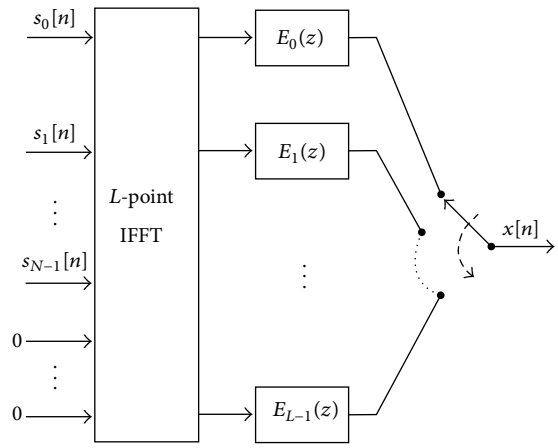

Figure 14: Basic synthesis polyphase filter bank.

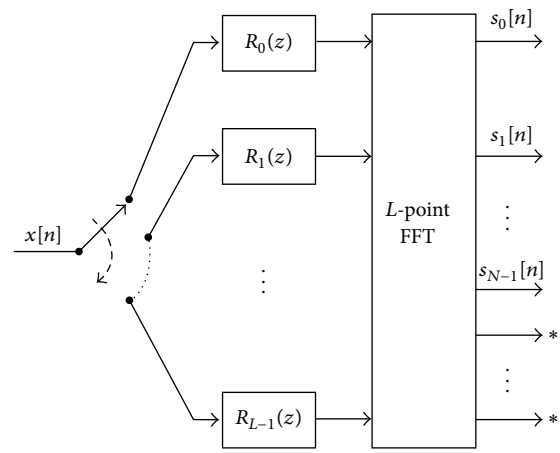

Figure 15: Basic analysis polyphase filter bank.

and, hence, facilitate additional filtering in the further stages of the transmitter.

(4) The filtering blocks $E_0(z)$ through $E_{L-1}(z)$ are the polyphase components of the prototype filter $p[n]$.

(5) This structure is an efficient implementation of a bank of filters with the respective inputs $s_0[n], s_1[n], \ldots, s_{N-1}[n]$ and the transfer functions $P(e^{j2\pi f})$, $P(e^{j2\pi(f-1/L)}), \ldots, P(e^{j2\pi(f-(N-1)/L)})$, where $P(e^{j2\pi f})$ is the Fourier transform of $p[n]$.

(6) The commutator at the output serializes the outputs of the polyphase component filters, after arrival of each set of data symbols at the input.

Figure 15 presents the basic polyphase AFB that matches with the SFB of Figure 14. Here, $R_k(z) = E_{L-k-1}(z)$. In the literature, $E_k(z)$ and $R_k(z)$ are distinguished by referring to them as type I and type II polyphase components [49]. When $x[n]$ is fed to its input, within the accuracy provided by the prototype filter $p[n]$, the data sequences $\{s_k[n], k = 0, 1, \ldots, N-1\}$ appear at its first N outputs. In other word, if $x[n]$ is passed through an ideal channel (free of distortion and noise), the SFB may be used to recover the transmitted data symbols $s_k[n]$. Obviously, channel introduces distortion and thus the AFB outputs should pass through a bank of equalizers to recover the data symbols $s_k[n]$.

5.2. Polyphase Structures for CMT and SMT. CMT and SMT systems, as was demonstrated in Section 3, are effectively the same modulations. For instance, a CMT waveform can be generated using an SMT waveform generator and subsequently apply a positive spectral shift of one half of the subcarrier spacing to the result. Alternatively, an SMT waveform may be generated using a CMT waveform generator and subsequently apply a negative spectral shift of one half of the subcarrier spacing to the result. It turns out that the development of structures for SMT waveform is more straightforward than those of the CMT. We thus continue this section with development of a pair of transmitter and receiver structures for SMT. The relevant CMT structures will follow through simple modifications of the SMT structures following the details provided in Section 3.

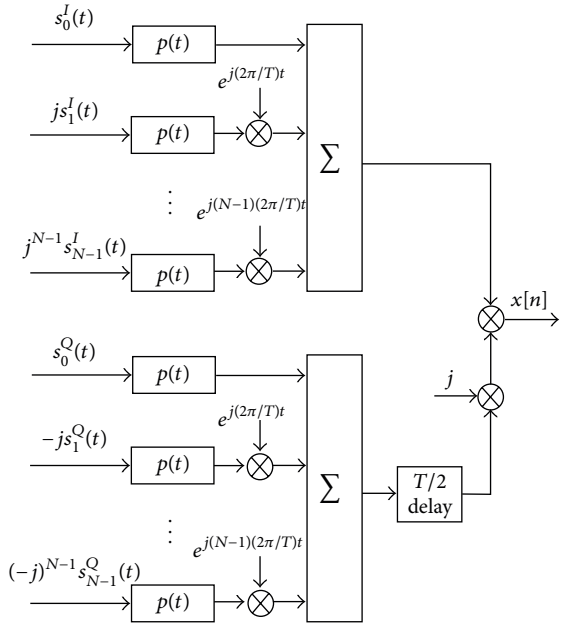

Figure 16: A rearrangement of the transmitter of SMT.

(1) SMT Transmitter. To develop a computationally efficient polyphase structure for SMT transmitter, we begin with rearranging the transmitter part of Figure 6 as in Figure 16. This, clearly, is obtained by separating the phase and quadrature parts of the SFB, combining the phase shifts at different points in the structure and adding the combined results to the real data symbols, $s_k^I[n]$ and $s_k^Q[n]$, at the input. The delay of $T/2$ in the prototype filters in the quadrature paths has been shifted to the corresponding filter bank output.

The structure that is presented in Figure 16 consists of a pair for SFBs. Clearly, each of these filter banks may be implemented efficiently using the basic polyphase structure of Figure 14. This implementation is presented in Figure 17.

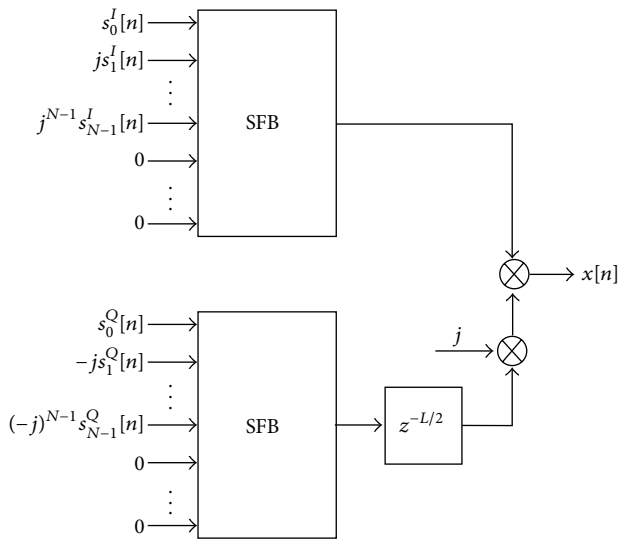

Figure 17: A rearrangement of the transmitter of SMT.

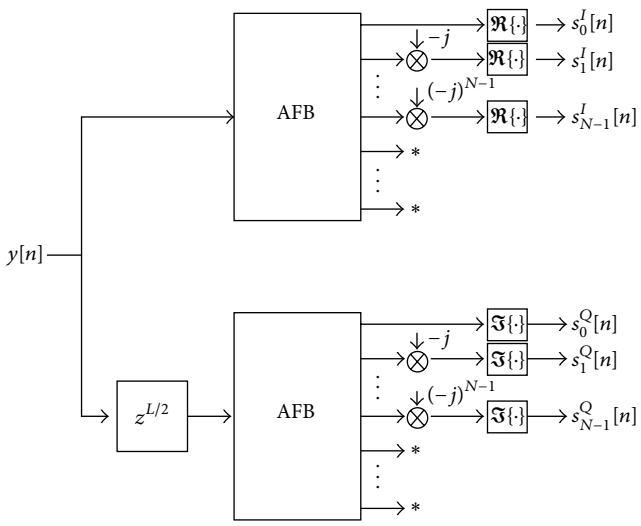

Figure 18: A rearrangement of the receiver of SMT.

It involves two separate polyphase structures. However, a closer look at the inputs to the polyphase structures reveals that they are modulated versions of two real vectors:

$$\mathbf{s}^I[n] = \left[s_0^I[n] \;\; s_1^I[n] \;\; \cdots \;\; s_{N-1}^I[n] \;\; 0 \;\; \cdots \;\; 0\right]^T,$$
$$\mathbf{s}^Q[n] = \left[s_0^Q[n] \;\; \cdots \;\; s_{N-1}^Q[n] \;\; 0 \;\; \cdots \;\; 0\right]^T. \tag{37}$$

As demonstrated next, one may take advantage of this property to combine the two SFBs into one.

Looking back at the synthesis polyphase structure of Figure 14, it may be argued that one can start with the real vectors $\mathbf{s}^I[n]$ and $\mathbf{s}^Q[n]$ at the input to the IFFT block and apply the modulation effect at the output of the IFFT through a circular rotation of the results. In that case, one may start with the computation of IFFT of the real vectors $\mathbf{s}^I[n]$ and $\mathbf{s}^Q[n]$. It is well known that this pair of IFFTs can be implemented through a single IFFT with a computational complexity of $(L/2)\log_2 L$ complex multiplications. On the other hand, we note that since the coefficients of the prototype filter $p[n]$ are real-valued, the complexity of implementation of two sets of polyphase component filters in Figure 17 involves $2\beta L$ real by complex multiplications, equivalent to βL complex multiplications. Adding these results, the total complexity of the SMT transmitter is measured as $(L/2)\log_2 L + \beta L$ complex multiplications per each set of complex output symbols. Recall that the length of the prototype filter $p[n]$ was assumed to be equal $\beta L + 1$. Here, we have replaced this by βL for brevity of the expressions. Also, we are only counting the number of multiplications as the measure of complexity. This is because, in practice, each multiplication is usually followed by an addition. Hence, without involving ourselves with details, we argue that the number of additions in each implementation is about the same as the number of multiplications.

It is also worth noting that a number of other authors also have taken note of the same symmetry properties in SMT waveform and accordingly proposed methods of reducing the complexity [73–75]. All these works have reached the complexity numbers that are similar to those presented here.

(2) SMT Receiver. In the absence of channel, the analysis of an SMT signal at the receiver can be performed with the same complexity as its synthesis counterpart at the transmitter [74, 75]. However, the presence of the channel destroys the symmetry property of SMT waveform. Hence, the implementation approach used at the transmitter cannot be extended to the receiver. In particular, we note that although the final goal is to extract the real-valued data symbols, the analyzed signals are the preequalized ones and, hence, are complex-valued.

Following the same line of thoughts that led to Figure 17, the receiver side of Figure 6 can be rearranged as in Figure 18, where the AFB blocks follow the structure presented in Figure 15. This structure, yet, does not include the channel equalizers that should be added at each output branch. Also, as noted in the previous section, the equalizers may be single-tap or multitap. Furthermore, one may note that since the pair of AFBs in Figure 18 are the same, but separated by $L/2$ sample delay, they may be combined as one AFB. Moreover, the phase rotations $(-j)^k$ at the output side may be absorbed in the equalizers. Combining these points, we arrive at the SMT receiver structure presented in Figure 19.

The receiver structure presented in Figure 19 has a complexity of one AFB plus N equalizers for each set of real symbols, $s_k^I[n]$ or $s_k^Q[n]$. Assuming that each equalizer has M complex tap weights, and noting that at each equalizer output we need either the real or imaginary part of the result, the total complexity of the receiver structure of Figure 19 is obtained as $(L/2)\log_2 L + (MN + KL + 1)/2$ complex multiplications per each set of real output symbols.

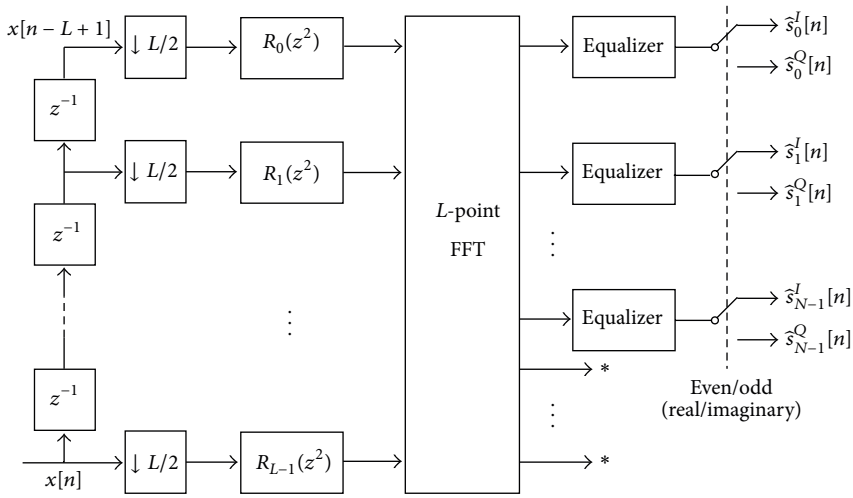

Figure 19: SMT receiver structure. The equalizers are single-tap or multitap. When they are multitap, they have a tap spacing of half a symbol interval.

Alternatively, we may say the total complexity of the receiver structure of Figure 19 is $L\log_2 L + MN + KL + 1$ complex multiplications per each set of complex output symbols.

5.3. Polyphase Structures for FMT. The polyphase SFB that is presented in Figure 14 implements a bank of synthesis filters whose center frequencies are at the normalized frequencies $0, 1/L, 2/L, \ldots$, equivalent to the unnormalized frequencies $0, 1/T, 2/T, \ldots$, respectively. Also, the sampling rate at the SFB output is $f_s = L/T$. Equivalently, the sampling interval at the SFB output is $T_s = T/L$. The same is true for the AFB that is presented in Figure 15.

In FMT, the situation is different. While the symbol rate remains equal to $1/T$, each subcarrier bandwidth and accordingly the FMT waveform bandwidth increase by a factor of $1 + \alpha$. Therefore, the sampling frequency of the synthesized waveform should be increased to $f_s = L(1+\alpha)/T$. This, in turn, implies that $T_s = T/(L(1+\alpha))$, and accordingly, in discrete-time, data symbols at the SFB input should be up-sampled $K = L(1+\alpha)$ fold (it is assumed that α is chosen such that K will be an integer number). Similarly, at the receiver side, the output of the AFB should be decimated K fold. Nevertheless, it should be noted that the center frequency of subcarriers remains unchanged; that is, it will be at 0, $1/L$, $2/L, \ldots$.

The fact that $K \neq L$ introduces some irregularity in the polyphase components which needs a special care. Most of the work in the literature that have addressed this issue have looked at the samples of underlying continuous time and accordingly have discussed how the corresponding polyphase filter bank should be implemented. This treatment, unfortunately, has led to a set of equations that are often hard to follow. Here, we present a solution that directly works with sampled signals/sequences [34]. This solution that has been presented for the first time in [72] is believed to be easier to follow. Here, we quote our original formulation from [72].

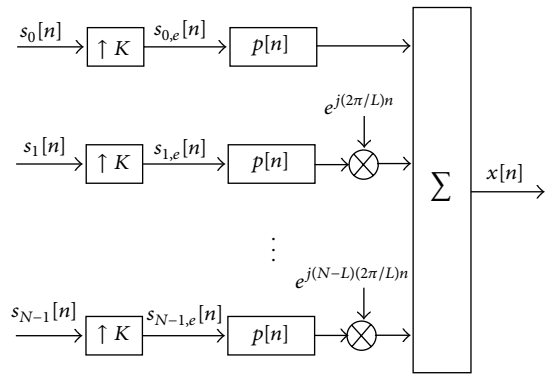

Figure 20: FMT transmitter in discrete-time.

(1) FMT Transmitter. Figure 20 presents a discrete-time equivalent of the SFB of Figure 7. Following this figure, one obtains

$$x[n] = \sum_{k=0}^{N-1} \left(\sum_m s_k[m]\, p[n - mK] \right) e^{j(2\pi kn/L)} = \sum_m \left(\sum_{k=0}^{N-1} s_k[m]\, e^{j(2\pi kn/L)} \right) p[n - mK]. \quad (38)$$

To proceed, we write the time index n as

$$n = \gamma L + \ell, \quad (39)$$

where γ is the integer part of n/L and $\ell = 0, 1, \ldots, L-1$, is the remainder of n/L. Similarly, n may be written as

$$n = \eta K + \kappa, \quad (40)$$

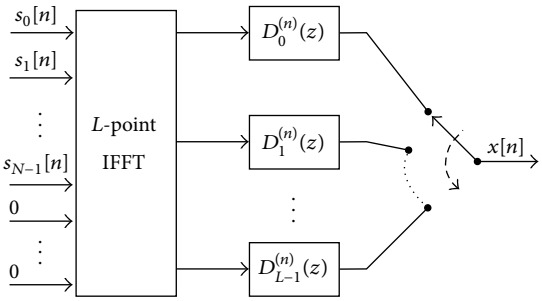

Figure 21: Polyphase implementation of an FMT transmitter.

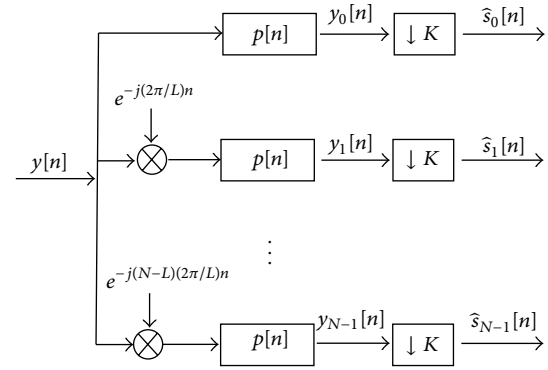

Figure 22: FMT receiver in discrete-time.

where η is the integer part of n/K and $\kappa = 0, 1, \ldots, K-1$ is the remainder of n/K. Next, we use (39) to substitute for n in the exponential term in (38) to obtain

$$S_\ell[m] = \sum_{k=0}^{N-1} s_k[m]\, e^{j(2\pi k\ell/L)}, \tag{41}$$

where we have noted that $e^{j(2\pi kn/L)} = e^{j(2\pi k\ell/L)}$. We may also note that $S_\ell[m]$ is the L-point IFFT of input symbols $s_0[n], s_1[n], \ldots, s_{N-1}[n]$ for $n = m$. Using (41) and substituting (40) into (38), we obtain

$$x[\eta K + \kappa] = \sum_m S_\ell[m]\, p[(\eta - m)K + \kappa], \quad \kappa = 0, 1, \ldots, K-1. \tag{42}$$

Equation (42) may be interpreted and accordingly implemented as follows. For each set of input symbols $s_0[n], s_1[n], \ldots, s_{N-1}[n]$, K samples of $x[n]$ are calculated. This calculation begins with performing an L-point IFFT on the input symbols $s_0[n], s_1[n], \ldots, s_{N-1}[n]$. The output samples from the IFFT are passed through the polyphase components of the prototype filter $p[n]$, where the polyphase components are with respect to the decimation factor K. This process is depicted in a block diagram form in Figure 21. The commutator at the output of Figure 21 takes K steps after arrival of each set of input symbols. $D_0^{(n)}(z)$ through $D_{L-1}^{(n)}(z)$ are a set of time-varying filters that are picked up from the set of K polyphase components $E_0(z)$ through $E_{K-1}(z)$ of the prototype filter $P(z) = \sum_n p[n]z^{-n}$. For a given time n, $x[n]$ is taken from the output of $D_\ell^{(n)}(z)$ and $D_\ell^{(n)}(z) = E_\kappa(z)$, where ℓ and κ are the integers defined according to (39) and (40), respectively.

Following Figure 21, the complexity of implementation of FMT transmitter, for each set of data symbols, is obtained as $(L/2)\log_2 L + \beta L$ complex multiplications.

(2) FMT Receiver. Following the same line of arguments that led to Figure 20, the discrete-time implementation of an FMT receiver is obtained as in Figure 22. From this figure, it follows that, for $k = 0, 1, \ldots, N-1$,

$$y_k[n] = \left(y[n]\, e^{-j(2\pi kn/L)}\right) \star p[n] = \sum_m y[m]\, e^{-j(2\pi km/L)}\, p[n-m]. \tag{43}$$

To proceed, we define

$$m = \gamma L + \ell, \tag{44}$$

where γ is the integer part of m/L and $\ell = 0, 1, \ldots, L-1$, is the remainder part of m/L. Using (44), (43) may be rearranged as

$$y_k[n] = \sum_\gamma \sum_{\ell=0}^{L-1} y[\gamma L + \ell]\, e^{-j(2\pi k\ell/L)}\, p[n - \gamma L - \ell] = \sum_{\ell=0}^{L-1} \left(\sum_\gamma y[\gamma L + \ell]\, p[n - \gamma L - \ell] \right) e^{-j(2\pi k\ell/L)}. \tag{45}$$

According to Figure 22, the recovered symbol $\widehat{s}_k[n]$ is obtained after K-fold decimation of $y_k[n]$. Moreover, in practice, a timing recovery loop determines a timing phase at which $y_k[n]$ should be decimated. Equalization is also necessary to combat the distortion introduced by the channel. A single-tap or a multitap equalizer per subcarrier may be used. In the latter case, one may use a fractionally spaced equalizer to relax on the sensitivity of the FMT receiver to timing phase. In such cases, the decimation factor is smaller than K.

Here, we present a general polyphase structure for computation of the samples of $y_k[n]$, for an arbitrary value of n; hence, any arbitrary choice of decimation factor is made possible. To this end, we write

$$n - \ell = \eta L + \kappa, \tag{46}$$

where η is the integer part of $(n-\ell)/L$ and $\kappa = 0, 1, \ldots, L-1$, is the remainder of $n - \ell$ divided by L. Using (46) into (45), we get

$$y_k[n] = \sum_{\ell=0}^{L-1} \left(\sum_\gamma y[\gamma L + \ell]\, p[(\eta - \gamma)L + \kappa] \right) e^{-j(2\pi k\ell/L)}. \tag{47}$$

Following (47), one may propose the analysis polyphase structure that is presented in Figure 23. The commutator takes the successive samples of the received signal $y[n]$ and distributes them across the inputs of the time-varying filters

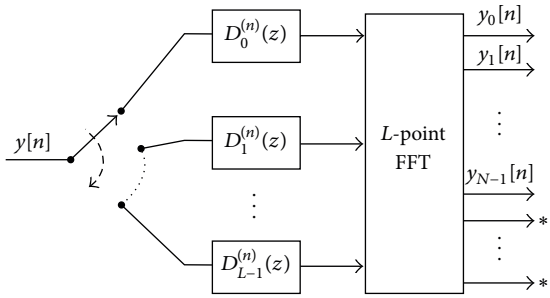

Figure 23: Polyphase implementation of an FMT receiver.

$D_0^{(n)}(z)$ through $D_{L-1}^{(n)}(z)$. The filters $D_0^{(n)}(z)$ through $D_{L-1}^{(n)}(z)$ are picked up from the set of L polyphase components $E_0(z)$ through $E_{L-1}(z)$ of the prototype filter $P(z) = \sum_n p[n]z^{-n}$. For a given time n, $D_\ell^{(n)}(z) = E_\kappa(z)$. The reader should be reminded that while in Figure 21 the time-varying filters $D_0^{(n)}(z)$ through $D_{L-1}^{(n)}(z)$ are picked up from the polyphase components of $P(z)$ with respect to the decimation factor K, in Figure 23 $D_0^{(n)}(z)$ through $D_{L-1}^{(n)}(z)$ are picked up from the polyphase components of $P(z)$ with respect to the decimation factor L.

Following Figure 23, the complexity of implementation of FMT receiver, for computation of each set of output samples, is obtained as $(L/2)\log_2 L + \beta L$ complex multiplications. In FMT, unlike CMT and SMT, the use of symbol spaced multitap equalizer is sufficient. If an M tap symbol spaced equalizer is used, one will find the complexity number $(L/2)\log_2 L + \beta L + MN$ complex multiplications per each set of detected data symbols.

5.4. Complexity Comparison with OFDM. Being an alternative to the widely adopted OFDM in various standards, it is always of interest and important to compare FBMC methods against OFDM. As noted in Section 1, the much higher quality of the prototype filter in FBMC makes it an ideal choice for many applications where OFDM faces challenges because of the poor frequency response of its prototype filter. Here, we discuss the additional complexity brought to FBMC (compared to OFDM) because of the use of a higher quality prototype filter.

We count the complexity of OFDM as one IFFT, $(L/2)\log_2 L$ complex multiplications, at the transmitter, and one FFT and N single-tap equalizers, $(L/2)\log_2 L + N$ complex multiplications, at the receiver. Thus, recalling the complexity numbers that were presented above, one finds that

$$\rho_{\text{SMT}}^{Tx} = \frac{\log_2 L + 2\beta}{\log_2 L}, \tag{48}$$

$$\rho_{\text{SMT}}^{Rx} = \frac{L\log_2 L + \beta L + MN}{(L/2)\log_2 L + N}, \tag{49}$$

where ρ_{SMT}^{Tx} and ρ_{SMT}^{Rx}, respectively, denote the relative complexity of SMT transmitter and receiver against OFDM. These numbers remain about the same in the case of CMT. To get a better feel of these complexity ratios in practical cases, consider a case where $L = 1024$, $N = 0.8L$ (i.e., 20% of subcarriers are left as guard band), $M = 1$, and $\beta = 4$. For this case, we find $\rho_{\text{SMT}}^{Tx} = 1.8$ and $\rho_{\text{SMT}}^{Rx} = 2.55$. For $M = 3$, the most likely value of M if a multitap equalizer is used, $\rho_{\text{SMT}}^{Rx} = 2.83$. Hence, one may say, CMT and SMT have a complexity that is roughly two to three times that of the OFDM.

Similarly, for FMT, we find that

$$\rho_{\text{FMT}}^{Tx} = \frac{\log_2 L + 2\beta}{\log_2 L}, \tag{50}$$

$$\rho_{\text{FMT}}^{Rx} = \frac{(L/2)\log_2 L + \beta L + MN}{(L/2)\log_2 L + N}. \tag{51}$$

Comparing (48) and (50), one will find that SMT/CMT and FMT transmitters have the same complexity. On the other hand, comparing (49) and (51), one will find that FMT receiver has a lower complexity than SMT/CMT. In any case, it still remains fair to say FBMC systems, in general, are two to three times more complex than OFDM. Nevertheless, it should be noted that this comparison is with a basic OFDM. It does not consider the cases where advanced signal processing methods may have to be adopted to compensate for other channel effects, for example, carrier frequency offset among different users in an OFDMA network. In such cases, one often finds that OFDM is more complex than FBMC [10].

6. Equalization

In FBMC receivers, equalization is performed at the output of the analysis filter banks. It is often assumed that each subcarrier has a small bandwidth; hence, the channel may be assumed to be flat over each subcarrier band. In that case, a single-tap equalizer per subcarrier would suffice. In cases where the flat gain approximation may be insufficient, a multitap equalizer per subcarrier band may be necessary. For CMT and SMT systems, it is necessary to use a fractionally spaced equalizer. A tap-spacing of half symbol interval is the most convenient choice and, hence, has been suggested in the literature, for example, [43]. FMT on the other hand allows the use of symbol spaced equalizers.

Although, in many scenarios it may appear that a single-tap equalizer per subcarrier is sufficient, in practice, where carrier and clock mismatch between the transmitter and receiver is inevitable, a multitap equalizer can be instrumental. In particular, the difference between the clock used at transmitter to pass the signal samples to a digital-to-analog converter (DAC) and the one used at the receiver to control the rate of samples taken by an analog-to-digital converter (ADC) at the receiver introduces a constant drift in the timing phase of sampled signal. This drift, as explained in the next section, can significantly deteriorate the receiver performance. The use of a multitap equalizer can resolve this problem to a great extent. This is demonstrated through a numerical example in the next section.

Another point that should be emphasized here is the following. Most researchers, who have published in the area

of FBMC, have limited their results to the use of one single-tap equalizer per subcarrier band. This has been to emphasize on the simplicity of equalization in FBMC systems and also to stay in par with OFDM. Alternatively, one may look at the use of multitap equalizers in FBMC systems as a mechanism that brings with itself a number of advantages. Firstly, the use of multitap equalizers removes any small frequency selectivity over each subcarrier band and, hence, facilitates adoption of a large symbol constellations and this, in turn, increases the bandwidth efficiency of transmission. Secondly, it allows reducing the number of subcarriers which, in turn, reduces the system (i) complexity (possibly compensating for the added complexity resulting from the use of multitap equalizers), (ii) latency, (iii) sensitivity to carrier frequency offset, and (iv) peak-to-average power ratio (PAPR).

7. Synchronization and Tracking Methods

Synchronization methods are necessary in any receiver to compensate for any difference between the carrier frequency of the incoming signal and the local oscillator used to demodulate it as well as to compensate for any clock mismatch between the transmitter and receiver. Pilot aided and blind synchronization methods have been widely studied in the literature from the beginning of development of data modems [76].

In majority of standards, including those of OFDM and FBMC, the pilot aided approaches have been adopted. For instance, all the OFDM packet formats that have been proposed for WiFi and WiMAX as well as those suggested in LTE and LTE-Advanced start with a short-training periodic preamble, for coarse carrier acquisition. This follows by a long preamble, consisting of two or more similar OFDM symbols, that is used for fine tuning of the carrier, timing acquisition, and channel estimation; for example, see [72, 77]. In addition, to be able to track channel variations during the payload of each packet, it is often proposed to insert distributed pilots in the time-frequency space. Interpolation methods are then used to obtain the channel gain and accordingly the equalizers gain, at the data points [78–81].

A few researchers, who have looked at the packet design for FBMC, have also suggested a similar packet format to those of the OFDM [82–86]. In particular, a periodic training consisting of a few repetitions of a pilot FBMC symbol is suggested to be used along with a least squares or a maximum likelihood estimator to estimate CFO and symbol timing. This is equivalent to long preamble in OFDM. Moreover, in [82], it is noted that the use of a short preamble, similar to that of OFDM, may be useful for coarse estimation of carrier, so that fine tuning of carrier and timing phase based on the long preamble can be established more robustly. Distributed pilots to track channel variations in payload part of FBMC packets have also been proposed [87, 88]. In the rest of this section, we make comments/suggestions for future research in three directions related to synchronization and tracking methods in FBMC systems.

7.1. Preamble Design. Figure 24 presents the packet format that has been proposed in [82–86]. The short preamble consists of a few tones with wider separation than the subcarrier spacing to allow detection of large CFO values. It is used to obtain a coarse estimate of CFO, so that the residual CFO (after removal of the estimated CFO) will be within the range of half symbol spacing. The long preamble, then, may be used for fine tuning of the carrier. The works presented in [83–85] do not mention the short preamble, but they make assumption that CFO is within the range of half symbol spacing. Naturally, to satisfy this assumption a mechanism similar to short preamble may be necessary.

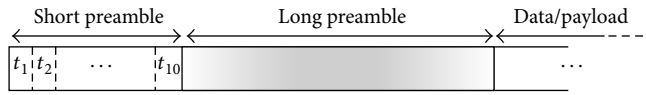

Figure 24: An FBMC data packet with short and long preambles.

There is also some difference in the long preamble proposed in [83–85] and the one proposed in [82, 86]. In the context of SMT waveform, the long preamble proposed in [83–85] is constructed based on a set of complex-valued pilot symbols that occupy all subcarriers. The long preamble proposed in [82, 86], on the other hand, is real-valued and only occupies the alternate subcarriers; the other subcarriers are left empty. This modification/simplification of the long preamble as demonstrated through numerical results in [86] improves the accuracy of the CFO estimates significantly.

Here, to make suggestions to further improve the preamble design, we first note that the preamble is a packet component that constitutes a loss in the bandwidth efficiency of transmission. Clearly, an attempt to reduce the length of the preamble improves the bandwidth efficiency. The research so far in the above cited works has led to the following observations. (i) A preamble with a set of pilot symbols that are well separated in frequency is needed to assure detection and correction of large CFO values. (ii) A longer preamble that allows a more accurate estimate of CFO may be also necessary. On the other hand, one may realize that to obtain the CFO and symbol timing estimates, it is not necessary to send pilots on all the subcarriers. The number of parameters that characterize the channel response (determined by the length of the channel impulse response) is usually much smaller than the number of subcarriers. This means, a fraction of subcarriers, whose number is greater than or equal to the length of the channel impulse response, suffice for pilot subcarriers in the preamble. This, in turn, implies that one may propose to combine the short and long preambles into one preamble, and by taking such approach, obviously, a shorter preamble will result. We note that the preamble proposed in [82, 86], compared to those proposed in [83–85], may be viewed as a step forward in this direction. While the works in [83–85] use all subcarriers to transmit the preamble pilots, [82, 86] allocate pilots only to alternate (even or odd) subcarriers.

Another consideration that needs one's attention in designing an effective preamble is the choice of the prototype filter that is used for preamble. Assuming that the preamble consists of only a long preamble, the preamble length is determined by the length of the prototype filter and the

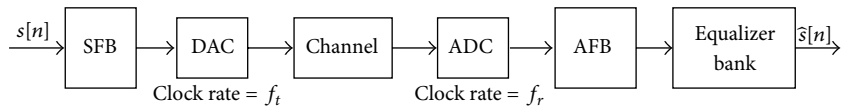

Figure 25: An FBMC transceiver with timing drift and the corresponding compensator block.

number of its repetitions. Accordingly, a shorter prototype filter leads to a shorter preamble and thus a more bandwidth efficient packet. The above suggestion to space out the pilot subcarriers in the preamble can be taken advantage of to shorten the length of the preamble. This is because wider subcarrier allows one to increase the bandwidth of each subcarrier and accordingly reduce the symbol period and thus the length of the corresponding prototype filter. Nevertheless, it should be also noted that a broader band of each subcarrier can make it prone to some level of frequency selectivity that should be taken into account while identifying the channel parameters.

7.2. Channel Tracking. Tracking of channel variation (including variations due to CFO and clock timing drift), during the payload transmission, is usually made through distributed pilots that are transmitted along with the data symbols. This topic, as noted above, has been well studied for OFDM. However, it has received very limited attention in the FBMC literature. Stitz et al. [88] have studied the problem of pilot-aided synchronization and tracking methods in CMT/SMT-type systems. They have shown that by applying specific pilots designed for CMT/SMT, the carrier frequency offset (CFO), fractional time delay (FTD), and channel response can be accurately estimated. The work presented in [89] has taken a different approach. It takes note of the fact that each signal component at the output of the analysis filter bank, before performing equalization and taking its real (or imaginary) part, has the form of $h_k[n](s_k[n] + j\psi_k[n])$ (or $h_k[n](js_k[n] + \psi_k[n])$), where $\psi_k[n]$ arises from ICI and ISI. It is thus argued that if the same (known) symbol is transmitted over two instants of times at the same subcarrier or allocated to the real and imaginary parts of an OQAM symbol in a SMT waveform, the analyzed signal samples give a pair of equations that can be solved to obtain an estimate of $h_k[n]$.

In [27] (also see [90]), it has been noted that the use of PAM symbols in CMT (and similarly in SMT, if the real and imaginary parts of each OQAM symbol are viewed as a pair of PAM symbols) allows development of a blind equalization algorithm. This algorithm may also be used for channel tracking. Hence, in CMT and SMT channel tracking is possible without any use of pilot symbols. To elaborate more on this possibility, we note that the convergence behavior of the blind equalizer that is developed in [27] was thoroughly analyzed in [91] (also see [92, 93]). It was found that the CMT/SMT blind equalizer has a well-behaved performance surface around its optimal setting. This implies that if the equalizer gain is set near its optimal value and channel subsequently varies slowly, the blind equalization algorithm of [27] can easily track the channel variation. This observation that yet to be thoroughly studied will add an additional advantage to CMT and SMT over OFDM in terms of bandwidth efficiency.

7.3. Timing Tracking. As noted above, any difference between the clock frequency at the transmitter and its counterpart at the receiver introduces a timing drift. The common method of compensating for this timing drift is to add a timing recovery loop to the system. In a single carrier receiver, the addition of a timing recovery loop as part of the receiver processing is a relatively straightforward task and is well understood [72, 94]. In an OFDM system, with a not very long payload, the timing drift may be absorbed by the CP, provided that not the full length of the CP has been consumed by the channel transient response. Drift of timing phase introduces a linear phase across frequency and that can be easily compensated by the single-tap equalizers at the FFT outputs. In FBMC, on the other hand, the absence of CP/guard interval makes an FBMC receiver more sensitive to timing drift. However, fortunately, this problem can be resolved trivially through the use of a set of multitap fractionally spaced equalizers, one per subcarrier.

To demonstrate the impact of per subcarrier fractionally spaced equalizers on resolving the problem of timing drift, we consider a CMT/SMT transceiver system which we simulate following the schematic diagram presented in Figure 25. The samples of the transmit signal are converted from digital to analog using a DAC that operated at a clock rate of f_t. At the receiver, the received signal is sampled through an ADC with a clock that has a rate of f_r. The clock frequencies f_t and f_r are different but typically are close. In practice, their difference may be as large as 50 ppm (part per million). This corresponds to the case where each clock has a precision of 25 ppm.

For the purpose of demonstration here, we consider the case where channel is absent. In that case, the effect of using a pair of DAC and ADC with different clock rates is like resampling the generated waveform with a resampling ratio f_r/f_t. This concept can be easily applied in a MATLAB simulation environment that we use, using the function "resample." The results of simulating a CMT system with 64 active subcarriers and a clock drift of 50 ppm are presented in Figure 26. The results show the signal-to-interference ratio (SIR) averaged over all subcarriers, as one proceed over successive CMT symbols. Timing phase is set to zero (i.e., perfect timing) at the beginning. The drift of timing phase introduces some ISI that cannot be resolved when single-tap equalizers are used but can be compensated through multitap equalizers. Perfect compensation may require a long equalizer. However, a 3- or 5-tap equalizer is sufficient to avoid a significant drop of SIR. We consider an SIR of above 30 dB as acceptable, given that, in typical practice, communication systems are often designed for output SINR values 20 dB or less. A margin of 10 dB should be sufficient to consider ISI/ICI due to timing drift as negligible. For the numerical example presented here, while a single-tap equalizer can preserve the SIR of above 30 dB for the first 400 CMT symbols, the use of a 3-tap and

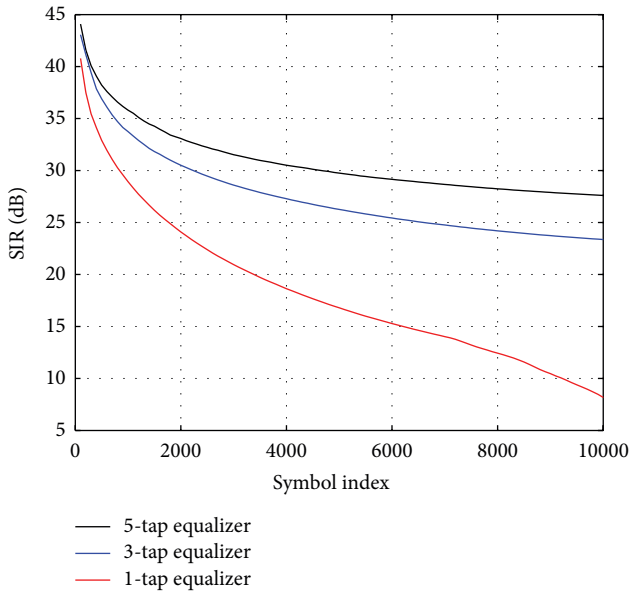

FIGURE 26: SIR variation as a function of symbol index (equivalently, timing drift) in a CMT transceiver.

5-tap equalizer increases this range to 1200 and 2500 CMT symbols, respectively.

Another possible solution that may be adopted to resolve the difference between the DAC clock at the transmitter and ADC clock at the receiver may be proposed by taking note of the following observation. An FBMC waveform (being CMT, SMT, or FMT) is a cyclostationary signal whose statistics are repeated every T_c second, where T_c is an integer multiple of the symbol period T. In FMT and SMT, $T_c = T$, and in CMT, $T_c = 2T$. We conjecture that taking note of this property, one can design a digital resampler circuit that may be added to the output of ADC, at the receiver, for tuning the number of samples per each period of T_c equal to a predefined value. Such solution is yet to be found through a clever study of the underlying signals.

8. Applications

In [19], OFDM and FBMC are contrasted with respect to their suitability for different applications. It is noted that while for many applications OFDM is a perfect choice, FBMC may be a superior choice for other applications. The applications in which FBMC may be preferred are (i) the uplink of multiuser multicarrier systems, (ii) cognitive radios, (iii) doubly dispersive channels, and (iv) digital subscriber lines and power line communications. Detailed discussion on why FBMC is a better choice in these applications is provided in [19]. The rest of this section emphasizes on an emerging class of communication systems, massive (multiuser) MIMO, whose significance as an enabling technology for 5G has recently been discussed in the literature and other forums.

Massive MIMO, in essence, is a multiuser technique, somewhat similar to code division multiple access (CDMA). In its simplest form, each mobile terminal (MT) has a single antenna, but the base station (BS) has a large number of antennas. The spreading code for each user is then the vector of channel gains between the respective MT antenna and the multiple antennas at the BS. Accordingly, by increasing the number of antennas at the BS, the processing gain of each user can be increased to an arbitrarily large value. In the pioneering work of Marzetta [95] it is noted that, in the limit, as the number of BS antennas tends to infinity, the processing gain of the system tends to infinity and, as a result, the effects of both noise and multiuser interference (MUI) are completely removed. Therefore, the network capacity (in theory) can be increased unboundedly by increasing the number of antennas at the BS [95].

Motivated by Marzetta's observations [95] multiple research groups in recent past have studied a variety of implementation issues related to massive MIMO systems, for example, [96–100]. Also, different groups have started the development of testbeds to confirm the theoretical observation of [95], in practice, for example. An assumption made by Marzetta [95] and followed by other researchers is that orthogonal frequency division multiplexing (OFDM) may be used to convert the frequency selective channels between each MT and the multiple antennas at the BS to a set of flat fading channels. Accordingly, the flat gains associated with the set of channels within each subcarrier constitute the spreading gain vector that is used for dispreading of the respective data in upstream as well as for precoding of the respective downstream data.

In a recent work [101], embarking on the above concepts, we have introduced the application of filter bank multicarrier (FBMC) to the area of massive MIMO communications. The interesting finding in this work is that unlike in conventional MIMO where applicability of FBMC (CMT and SMT, in particular) is found limited, FBMC offers a number of appealing properties in the application of massive MIMO. In particular, the linear combining of the signal components from different antennas at BS (equivalent to dispreading in CDMA) smooths channel distortion across each subcarrier band. This property, which we call *self-equalization*, allows one to relax on the requirement of having approximately flat gain for the subcarriers. This, in turn, allows one to reduce the number of subcarriers in an assigned bandwidth. Reducing the number of subcarriers has the following impacts, which all position FBMC as a strong candidate in the application of massive MIMO.

(1) The complexity of both transmitter and receiver will be reduced, since the underlying polyphase structures will be based on smaller size IFFT/FFT blocks.

(2) The system latency will be reduced. This is because the length and, thus, the corresponding group delay of the underlying prototype filter are reduced.

(3) The system sensitivity to CFO will be reduced.

(4) The PAPR of the transmit signal will be reduced.

The preliminary research results that are presented in [101], clearly, open up a new research direction for exploration of FBMC techniques in the area of massive MIMO.

9. Conclusions

This paper presented a tutorial review of the class of filter bank multicarrier (FBMC) communication systems, with emphasis on the recent results of the authors research laboratory. It was noted that by building FBMC systems based on well-designed prototype filters, the spectrum of each subcarrier can be contained within a limited bandwidth. This, in turn, allows transmission over noncontiguous bands, a property that makes FBMC an ideal choice for many applications, including the uplink of multiuser multicarrier networks and cognitive radios. It was also pointed out that FBMC systems can be adopted to doubly dispersive channels to achieve a performance far superior to that of OFDM. The polyphase structures that have been proposed for efficient implementation of FBMC systems were reviewed and their complexities were compared with that of a standard OFDM system. It was noted that the complexity of FBMC transmitters is close to (but less than) twice their OFDM counterpart, and the complexity of FBMC receivers is close to (but less than) three times that of their OFDM counterpart. However, it was also noted that, in some applications, for example, in the uplink of multiuser systems where synchronization cannot be made perfectly, hence, multiuser cancellation techniques should be applied, OFDM can be far more complex than FBMC. Moreover, it was noted that more research is needed to better understand the problems related to synchronization, equalization, and tracking of channel variations in FBMC systems. Possible application of FBMC in the emerging area of massive MIMO was also highlighted, and a number of advantages that FBMC offers in this application were identified.

Conflict of Interests

The author declares that there is no conflict of interests regarding the publication of this paper.

References

[1] W. Y. Chen, *DSL Simulation Techniques and Standards Development for Digital Subscriber Line Systems*, Macmillan Publishing, Indianapolis, Ind, USA, 1998.

[2] J. C. T. Starr and P. Silverman, *Understanding Digital Subscriber Line Technology*, Prentice Hall, Upper Saddle River, NJ, USA, 1999.

[3] R. V. Nee and R. Prasad, *OFDM for Wireless Multimedia Communications*, Arthec House, Boston, Mass, USA, 2000.

[4] Y. Li and G. Stüber, Eds., *Orthogonal Frequency Division Multiplexing for Wireless Communications*, Springer, New York, NY, USA, 2006.

[5] M. Morelli, C.-C. J. Kuo, and M.-O. Pun, "Synchronization techniques for orthogonal frequency division multiple access (OFDMA): a tutorial review," *Proceedings of the IEEE*, vol. 95, no. 7, pp. 1394–1427, 2007.

[6] D. Huang and K. B. Letaief, "An interference-cancellation scheme for carrier frequency offsets correction in OFDMA systems," *IEEE Transactions on Communications*, vol. 53, no. 7, pp. 1155–1165, 2005.

[7] K. Lee and I. Lee, "CFO compensation for uplink OFDMA systems with conjugated gradient," in *Proceedings of the IEEE International Conference on Communications (ICC '11)*, pp. 1–5, Kyoto, Japan, June 2011.

[8] K. Lee, S.-R. Lee, S.-H. Moon, and I. Lee, "MMSE-based CFO compensation for uplink OFDMA systems with conjugate gradient," *IEEE Transactions on Wireless Communications*, vol. 11, no. 8, pp. 2767–2775, 2012.

[9] A. Farhang, N. Marchetti, and L. E. Doyle, "Low complexity LS and MMSE based CFO compensation techniques for the uplink of OFDMA systems," in *Proceedings of the IEEE International Conference on Communications (ICC '13)*, pp. 5748–5753, IEEE, Budapest, Hungary, June 2013.

[10] H. Saeedi-Sourck, Y. Wu, J. W. M. Bergmans, S. Sadri, and B. Farhang-Boroujeny, "Complexity and performance comparison of filter bank multicarrier and OFDM in uplink of multicarrier multiple access networks," *IEEE Transactions on Signal Processing*, vol. 59, no. 4, pp. 1907–1912, 2011.

[11] S. Brandes, I. Cosovic, and M. Schnell, "Sidelobe suppression in OFDM systems by insertion of cancellation carriers," in *Proceedings of the 62nd IEEE Vehicular Technology Conference (VTC '05)*, vol. 1, pp. 152–162, September 2005.

[12] Z. Yuan, S. Pagadarai, and A. M. Wyglinski, "Cancellation carrier technique using genetic algorithm for OFDM sidelobe suppression," in *Proceedings of the Military Communications Conference (MILCOM '08)*, pp. 1–5, IEEE, 2008.

[13] A. Selim, I. Macaluso, and L. Doyle, "Efficient sidelobe suppression for OFDM systems using advanced cancellation carriers," in *Proceedings of the IEEE International Conference on Communications (ICC '13)*, pp. 4687–4692, Budapest, Hungary, June 2013.

[14] S. N. Premnath, D. Wasden, S. K. Kasera, B. Farhang-Boroujeny, and N. Patwari, "Beyond ofdm: best-effort dynamic spectrum access using filterbank multicarrier," in *Proceedings of the 4th International Conference on Communication Systems and Networks (COMSNETS '12)*, January 2012.

[15] S. N. Premnath, D. Wasden, S. K. Kasera, N. Patwari, and B. Farhang-Boroujeny, "Beyond OFDM: best-effort dynamic spectrum access using filterbank multicarrier," *IEEE/ACM Transactions on Networking*, vol. 21, no. 3, pp. 869–882, 2013.

[16] B. Farhang-Boroujeny and R. Kempter, "Multicarrier communication techniques for spectrum sensing and communication in cognitive radios," *IEEE Communications Magazine*, vol. 46, no. 4, pp. 80–85, 2008.

[17] B. Farhang-Boroujeny, "Prolate filters for nonadaptive multitaper spectral estimators with high spectral dynamic range," *IEEE Signal Processing Letters*, vol. 15, pp. 457–460, 2008.

[18] B. Farhang-Boroujeny, "Filter bank spectrum sensing for cognitive radios," *IEEE Transactions on Signal Processing*, vol. 56, no. 5, pp. 1801–1811, 2008.

[19] B. Farhang-Boroujeny, "OFDM versus filter bank multicarrier," *IEEE Signal Processing Magazine*, vol. 28, no. 3, pp. 92–112, 2011.

[20] A. Sahin, I. Guvenc, and H. Arslan, "A survey on multicarrier communications: prototype filters, lattice structures, and implementation aspects," *IEEE Communications Surveys and Tutorials*, vol. 16, no. 3, pp. 1312–1338, 2013.

[21] M. Bellanger, "FBMC physical layer: a primer," Tech. Rep. 06/2010, 2010.

[22] M. Payaró, A. Pascual-Iserte, and M. Nájar, "Performance comparison between FBMC and OFDM in MIMO systems under channel uncertainty," in *Proceedings of the European Wireless Conference (EW '10)*, pp. 1023–1030, April 2010.

[23] T. Ihalainen, A. Ikhlef, J. Louveaux, and M. Renfors, "Channel equalization for multi-antenna FBMC/OQAM receivers," *IEEE Transactions on Vehicular Technology*, vol. 60, no. 5, pp. 2070–2085, 2011.

[24] M. Tzannes, M. Tzannes, and H. Resnikoff, "The DWMT: a multicarrier transceiver for ADSL using M-band wavelet transforms," ANSI Contribution T1E1.4/93-067, 1993.

[25] M. Tzannes, M. Tzannes, J. Proakis, and P. Heller, "DMT systems, DWMT systems and digital filter banks," in *Proceedings of the IEEE International Conference on Communications (ICC '94)*, vol. 1, pp. 311–315, 1994.

[26] S. D. Sandberg and M. A. Tzannes, "Overlapped discrete multitone modulation for high speed copper wire communications," *IEEE Journal on Selected Areas in Communications*, vol. 13, no. 9, pp. 1571–1585, 1995.

[27] B. Farhang-Boroujeny, "Multicarrier modulation with blind detection capability using cosine modulated filter banks," *IEEE Transactions on Communications*, vol. 51, no. 12, pp. 2057–2070, 2003.

[28] S. Galli and O. Logvinov, "Recent developments in the standardization of power line communications within the IEEE," *IEEE Communications Magazine*, vol. 46, no. 7, pp. 64–71, 2008.

[29] F. Sjoberg, R. Nilsson, M. Isaksson, P. Odling, and P. Borjesson, "Asynchronous Zipper [subscriber line duplex method]," in *Proceedings of the IEEE International Conference on Communications (ICC '99)*, vol. 1, pp. 231–235, Vancouver, Canada, June 1999.

[30] "Very-high bit-rate digital subscriber lines (vdsl) metallic interface, part 3: technical specification of a multi-carrier modulation transceiver," Working Group R1E1.4, Document T1E1.4/2000-013R3, 2000.

[31] D. J. G. Mestdagh, M. R. Isaksson, and P. Ödling, "Zipper VDSL: A solution for robust duplex communication over telephone lines," *IEEE Communications Magazine*, vol. 38, no. 5, pp. 90–96, 2000.

[32] M. Nava and G. Ökvist, "The zipper prototype: a complete and flexible VDSL multicarrier solution," *IEEE Communications Magazine*, vol. 40, no. 12, pp. 92–105, 2002.

[33] R. Nilsson, F. Sjöberg, M. Isaksson, J. M. Cioffi, and S. K. Wilson, "Autonomous synchronization of a DMT-VDSL system in unbundled networks," *IEEE Journal on Selected Areas in Communications*, vol. 20, no. 5, pp. 1055–1063, 2002.

[34] G. Cherubini, E. Eleftheriou, and S. Ölçer, "Filtered multitone modulation for very high-speed digital subscriber lines," *IEEE Journal on Selected Areas in Communications*, vol. 20, no. 5, pp. 1016–1028, 2002.

[35] "Very high speed digital subscriber line transceivers 2 (VDSL2)," ITU-T Recommendation G.993.2, 2006.

[36] M. Bellec and P. Pirat, "OQAM performances and complexity," IEEE P802.22 Wireless Regional Area Network, 2006, http://www.ieee802.org/22/Meeting_documents/2006_Jan/index.html.

[37] "Wideband air interface isotropic orthogonal transform algorithm," Public Safety Wideband Data Standards Project Digital Radio Technical Standards, TIA Committee TR-8.5, 2003.

[38] B. Farhang-Boroujeny and C. Yuen, "Cosine modulated and offset QAM filter bank multicarrier techniques: a continuous-time prospect," *EURASIP Journal on Advances in Signal Processing*, vol. 2010, Article ID 165654, 16 pages, 2010.

[39] R. Chang, "High-speed multichannel data transmission with bandlimited orthogonal signals," *Bell System Technical Journal*, vol. 45, pp. 1775–1796, 1966.

[40] B. Saltzberg, "Performance of an efficient parallel data transmission system," *IEEE Transactions on Communication Technology*, vol. 15, no. 6, pp. 805–811, 1967.

[41] M. G. Bellanger and J. L. Daguet, "TDM-FDM transmultiplexer: digital polyphase and FFT," *IEEE Transactions on Communications*, vol. 22, no. 9, pp. 1199–1205, 1974.

[42] B. Hirosaki, "An analysis of automatic equalizers for orthogonally multiplexed QAM systems," *IEEE Transactions on Communications*, vol. 28, no. 1, pp. 73–83, 1980.

[43] B. Hirosaki, "An orthogonally multiplexed qam system using the discrete fourier transform," *IEEE Transactions on Communications*, vol. 29, no. 7, pp. 982–989, 1981.

[44] B. Le Floch, M. Alard, and C. Berrou, "Coded orthogonal frequency division multiplex," *Proceedings of the IEEE*, vol. 83, no. 6, pp. 982–996, 1995.

[45] G. Cariolaro and F. C. Vagliani, "OFDM scheme with a half complexity," *IEEE Journal on Selected Areas in Communications*, vol. 13, no. 9, pp. 1586–1599, 1995.

[46] P. Siohan and C. Roche, "Cosine-modulated filterbanks based on extended Gaussian functions," *IEEE Transactions on Signal Processing*, vol. 48, no. 11, pp. 3052–3061, 2000.

[47] B. Hirosaki, S. Hasegawa, and A. Sabato, "Advanced groupband data modem using orthogonally multiplexed QAM technique," *IEEE Transactions on Communications*, vol. 34, no. 6, pp. 587–592, 1986.

[48] S. Govardhanagiri, T. Karp, P. Heller, and T. Nguyen, "Performance analysis of multicarrier modulation systems using cosine modulated filter banks," in *Proceedings of the IEEE International Conference on Acoustics, Speech, and Signal Processing (ICASSP '99)*, vol. 3, pp. 1405–1408, March 1999.

[49] P. Vaidyanathan, *Multirate Systems and Filter Banks*, Prentice Hall, Englewood Cliffs, NJ, USA, 1993.

[50] N. J. Fliege, *Multirate Digital Signal Processing*, John Wiley & Sons, New York, NY, USA, 1994.

[51] N. J. Fliege, "Modified DFT polyphase SBC filter banks with almost perfect reconstruction," in *Proceedings of the IEEE International Conference on Acoustics, Speech, and Signal Processing (ICASSP '94)*, vol. 3, pp. III/149–III/152, Adelaide, Australia, April 1994.

[52] P. N. Heller, T. Karp, and T. Q. Nguyen, "A general formulation of modulated filter banks," *IEEE Transactions on Signal Processing*, vol. 47, no. 4, pp. 986–1002, 1999.

[53] T. Karp and N. J. Fliege, "Modified DFT filter banks with perfect reconstruction," *IEEE Transactions on Circuits and Systems II: Analog and Digital Signal Processing*, vol. 46, no. 11, pp. 1404–1414, 1999.

[54] R. Bregović and T. Saramaki, "A systematic technique for designing linear-phase FIR prototype filters for perfect-reconstruction cosine-modulated and modified DFT filterbanks," *IEEE Transactions on Signal Processing*, vol. 53, no. 8, part 2, pp. 3193–3201, 2005.

[55] S. Salcedo-Sanz, F. Cruz-Roldan, C. Heneghan, and X. Yao, "Evolutionary design of digital filters with application to subband coding and data transmission," *IEEE Transactions on Signal Processing*, vol. 55, no. 4, pp. 1193–1203, 2007.

[56] P. Siohan, C. Siclet, and N. Lacaille, "Analysis and design of OFDM/OQAM systems based on filterbank theory," *IEEE Transactions on Signal Processing*, vol. 50, no. 5, pp. 1170–1183, 2002.

[57] P. Amini, R.-R. Chen, and B. Farhang-Boroujeny, "Filterbank multicarrier communications for underwater acoustic channels," *IEEE Journal of Oceanic Engineering*, 2014.

[58] B. Farhang-Boroujeny, "A square-root Nyquist (M) filter design for digital communication systems," *IEEE Transactions on Signal Processing*, vol. 56, no. 5, pp. 2127–2132, 2008.

[59] K. W. Martin, "Small side-lobe filter design for multitone data-communication applications," *IEEE Transactions on Circuits and Systems II: Analog and Digital Signal Processing*, vol. 45, no. 8, pp. 1155–1161, 1998.

[60] S. Mirabbasi and K. Martin, "Overlapped complex-modulated transmultiplexer filters with simplified design and superior stopbands," *IEEE Transactions on Circuits and Systems II: Analog and Digital Signal Processing*, vol. 50, no. 8, pp. 456–469, 2003.

[61] M. Rossi, J.-Y. Zhang, and W. Steenaart, "Iterative least squares design of perfect reconstruction QMF banks," in *Proceedings of the Canadian Conference on Electrical and Computer Engineering (CCECE '96)*, pp. 762–765, May 1996.

[62] W. Kozek and A. F. Molisch, "Nonorthogonal pulseshapes for multicarrier communications in doubly dispersive channels," *IEEE Journal on Selected Areas in Communications*, vol. 16, no. 8, pp. 1579–1589, 1998.

[63] G. Matz, D. Schafhuber, K. Gröchenig, M. Hartmann, and F. Hlawatsch, "Analysis, optimization, and implementation of low-interference wireless multicarrier systems," *IEEE Transactions on Wireless Communications*, vol. 6, no. 5, pp. 1921–1930, 2007.

[64] G. Matz, H. Bolcskei, and F. Hlawatsch, "Time-frequency foundations of communications: concepts and tools," *IEEE Signal Processing Magazine*, vol. 30, no. 6, pp. 87–96, 2013.

[65] B. Boashash, Ed., *Time Frequency Signal Analysis and Processing: A Comprehensive Reference*, Elsevier, Oxford, UK, 2003.

[66] R. Haas and J.-C. Belfiore, "A time-frequency well-localized pulse for multiple carrier transmission," *Wireless Personal Communications*, vol. 5, no. 1, pp. 1–18, 1997.

[67] M. Alard, "Construction of a multicarrier signal," Patent WO 96/35278, 1996.

[68] P. Amini, R.-R. Chen, and B. Farhang-Boroujeny, "Filterbank multicarrier for underwater communications," in *Proceedings of the 49th Annual Allerton Conference on Communication, Control, and Computing (Allerton '11)*, pp. 639–646, September 2011.

[69] P. Amini, C. H. Yuen, R.-R. Chen, and B. Farhang-Boroujeny, "Isotropic filter design for MIMO filter bank multicarrier communications," in *Proceedings of the IEEE Sensor Array and Multichannel Signal Processing Workshop (SAM '10)*, pp. 89–92, October 2010.

[70] J. Du and S. Signell, "Classic OFDM systems and pulse shaping OFDM/OQAM systems," Tech. Rep., KTH—Royal Institute of Technology, Stockholm, Sweden, 2007.

[71] T. Strohmer and S. Beaver, "Optimal OFDM design for time-frequency dispersive channels," *IEEE Transactions on Communications*, vol. 51, no. 7, pp. 1111–1122, 2003.

[72] B. Farhang-Boroujeny, *Signal Processing Techniques for Software Radios*, Lulu, Raleigh, NC, USA, 2nd edition, 2009.

[73] Y. Dandach and P. Siohan, "FBMC/OQAM modulators with half complexity," in *Proceedings of the IEEE Global Telecommunications Conference (GLOBECOM '11)*, pp. 1–5, Houston, Tex, USA, December 2011.

[74] G. Cariolaro and F. C. Vagliani, "An OFDM scheme with a half complexity," *IEEE Journal on Selected Areas in Communications*, vol. 13, no. 9, pp. 1586–1599, 1995.

[75] L. Vangelista and N. Laurenti, "Efficient implementations and alternative architectures for OFDM-OQAM systems," *IEEE Transactions on Communications*, vol. 49, no. 4, pp. 664–675, 2001.

[76] J. S. R. W. Lucky and E. Weldon, *Principles of Data Communications*, McGraw-Hill, New York, NY, USA, 1965.

[77] E. H. Ong, J. Kneckt, O. Alanen, Z. Chang, T. Huovinen, and T. Nihtila, "IEEE 802.11ac: enhancements for very high throughput WLANs," in *Proceedings of the 22nd International Symposium on Personal, Indoor and Mobile Radio Communications (PIMRC '11)*, pp. 849–853, IEEE, September 2011.

[78] I. Barhumi, G. Leus, and M. Moonen, "Optimal training design for MIMO OFDM systems in mobile wireless channels," *IEEE Transactions on Signal Processing*, vol. 51, no. 6, pp. 1615–1624, 2003.

[79] M. Dong and L. Tong, "Optimal design and placement of pilot symbols for channel estimation," *IEEE Transactions on Signal Processing*, vol. 50, no. 12, pp. 3055–3069, 2002.

[80] D. Hu, L. Yang, Y. Shi, and L. He, "Optimal pilot sequence design for channel estimation in MIMO OFDM systems," *IEEE Communications Letters*, vol. 10, no. 1, pp. 1–3, 2006.

[81] C. K. Ho, B. Farhang-Boroujeny, and F. Chin, "Added pilot semi-blind channel estimation scheme for OFDM in fading channels," in *Proceedings of the IEEE Global Telecommunicatins Conference (GLOBECOM '01)*, vol. 5, pp. 3075–3079, November 2001.

[82] B. Farhang-Boroujeny and P. Amini, "Packet format design and decision directed tracking methods for filter bank multicarrier systems," *EURASIP Journal on Advances in Signal Processing*, vol. 2010, Article ID 307983, 2010.

[83] T. Fusco, A. Petrella, and M. Tanda, "Joint symbol timing and CFO estimation in multiuser OFDM/OQAM systems," in *Proceedings of the IEEE 10th Workshop on Signal Processing Advances in Wireless Communications (SPAWC '09)*, pp. 613–617, June 2009.

[84] T. Fusco, A. Petrella, and M. Tanda, "Data-aided symbol timing and CFO synchronization for filter bank multicarrier systems," *IEEE Transactions on Wireless Communications*, vol. 8, no. 5, pp. 2705–2715, 2009.

[85] M. Tanda, T. Fusco, and A. Petrella, "Joint symbol timing and CFO estimation for OFDM/OQAM systems in multipath channels," *Eurasip Journal on Advances in Signal Processing*, vol. 2010, Article ID 897607, 2010.

[86] H. Saeedi-Sourck, S. Sadri, Y. Wu, and B. Farhang-Boroujeny, "Near maximum likelihood synchronization for filter bank multicarrier systems," *IEEE Wireless Communications Letters*, vol. 2, no. 2, pp. 235–238, 2013.

[87] T. H. Stitz, A. Viholainen, T. Ihalainen, and M. Renfors, "CFO estimation and correction in a WiMAX-like FBMC system," in *Proceedings of the 10th IEEE Workshop on Signal Processing Advances in Wireless Communications (SPAWC '09)*, pp. 633–637, June 2009.

[88] T. H. Stitz, T. Ihalainen, A. Viholainen, and M. Renfors, "Pilot-Based synchronization and equalization in filter bank multicarrier communications," *EURASIP Journal on Advances in Signal Processing*, vol. 2010, article 9, Article ID 741429, 2010.

[89] M. Bellanger and T. Dao, "Multicarrier digital transmission system using an OQAM transmultiplexer," Granted patent, US7072412, 2006.

[90] B. Farhang-Boroujeny, "Discrete multitone modulation with blind detection capability," in *Proceedings of the Vehicular*

Technology Conference (VTC '02), vol. 1, pp. 376–380, IEEE, 2002.

[91] L. Lin and B. Farhang-Boroujeny, "Convergence analysis of blind equalizer in a filter-bank-based multicarrier communication system," *IEEE Transactions on Signal Processing*, vol. 54, no. 10, pp. 4061–4067, 2006.

[92] "Convergence an alysis of blind equalizer in a cosine modulated filter bank-based multicarrier communication system," in *Proceedings of the Workshop on Signal Processing Advances in Wireless Communications (SPAWC '03)*, pp. 368–372, IEEE, 2003.

[93] L. Lin and B. Farhang-Boroujeny, "Analytical study of the performance surface of blind equalizer in a cosine modulated multicarrier communication system," in *Proceedings of the IEEE International Conference on Acoustics, Speech, and Signal Processing (ICASSP '05)*, pp. IV337–IV340, March 2005.

[94] F. J. Harris and M. Rice, "Multirate digital filters for symbol timing synchronization in software defined radios," *IEEE Journal on Selected Areas in Communications*, vol. 19, no. 12, pp. 2346–2357, 2001.

[95] T. L. Marzetta, "Noncooperative cellular wireless with unlimited numbers of base station antennas," *IEEE Transactions on Wireless Communications*, vol. 9, no. 11, pp. 3590–3600, 2010.

[96] J. Hoydis, S. Ten Brink, and M. Debbah, "Massive MIMO in the UL/DL of cellular networks: how many antennas do we need?" *IEEE Journal on Selected Areas in Communications*, vol. 31, no. 2, pp. 160–171, 2013.

[97] J. Hoydis, C. Hoek, T. Wild, and S. Ten Brink, "Channel measurements for large antenna arrays," in *Proceedings of the International Symposium on Wireless Communication Systems (ISWCS '12)*, pp. 811–815, Paris, France, August 2012.

[98] J. Jose, A. Ashikhmin, T. L. Marzetta, and S. Vishwanath, "Pilot contamination and precoding in multi-cell TDD systems," *IEEE Transactions on Wireless Communications*, vol. 10, no. 8, pp. 2640–2651, 2011.

[99] X. Gao, O. Edfors, F. Rusek, and F. Tufvesson, "Linear precoding performance in measured very-large MIMO channels," in *Proceedings of the IEEE Vehicular Technology Conference (VTC Fall '11)*, pp. 1–5, IEEE, San Francisco, Calif, USA, September 2011.

[100] S. Payami and F. Tufvesson, "Channel measurements and analysis for very large array systems at 2.6 GHz," in *Proceedings of the 6th European Conference on Antennas and Propagation (EuCAP '12)*, pp. 433–437, March 2012.

[101] A. Farhang, N. Marchetti, L. Doyle, and B. Farhang-Boroujeny, "Filter bank multicarrier for massive MIMO," in *Proceedings of the IEEE International Conference on Vehicular Technology (VTC-Fall '14)*, Vancouver, Canada, September 2014.